Interacting Effects of Light and Iron Availability on the Coupling of Photosynthetic Electron Transport and CO$_2$-Assimilation in Marine Phytoplankton

Nina Schuback[1]*, Christina Schallenberg[2], Carolyn Duckham[1], Maria T. Maldonado[1], Philippe D. Tortell[1,3]

1 Departement of Earth, Ocean and Atmospheric Sciences, University of British Columbia, Vancouver, BC, Canada, 2 School of Earth and Ocean Sciences, University of Victoria, Victoria, BC, Canada, 3 Department of Botany, University of British Columbia, Vancouver, BC, Canada

* nschuback@eos.ubc.ca

Abstract

Iron availability directly affects photosynthesis and limits phytoplankton growth over vast oceanic regions. For this reason, the availability of iron is a crucial variable to consider in the development of active chlorophyll a fluorescence based estimates of phytoplankton primary productivity. These bio-optical approaches require a conversion factor to derive ecologically-relevant rates of CO$_2$-assimilation from estimates of electron transport in photosystem II. The required conversion factor varies significantly across phytoplankton taxa and environmental conditions, but little information is available on its response to iron limitation. In this study, we examine the role of iron limitation, and the interacting effects of iron and light availability, on the coupling of photosynthetic electron transport and CO$_2$-assimilation in marine phytoplankton. Our results show that excess irradiance causes increased decoupling of carbon fixation and electron transport, particularly under iron limiting conditions. We observed that reaction center II specific rates of electron transport (ETR$_{RCII}$, mol e- mol RCII^{-1} s^{-1}) increased under iron limitation, and we propose a simple conceptual model for this observation. We also observed a strong correlation between the derived conversion factor and the expression of non-photochemical quenching. Utilizing a dataset from in situ phytoplankton assemblages across a coastal – oceanic transect in the Northeast subarctic Pacific, this relationship was used to predict ETR$_{RCII}$: CO$_2$-assimilation conversion factors and carbon-based primary productivity from FRRF data, without the need for any additional measurements.

Introduction

The photosynthetic assimilation of inorganic CO$_2$ into organic carbon by marine phytoplankton accounts for almost half of total global primary productivity [1], and variations in

phytoplankton primary productivity can profoundly affect ecosystem dynamics and global climate (e.g. [2–5]). However, despite its recognized importance, it remains challenging to accurately quantify marine primary production at the temporal and spatial resolution needed to relate its variability back to external environmental conditions. In vast oceanic regions, the availability of iron (Fe) limits marine phytoplankton primary productivity [6–8]. This element plays a fundamental role in the photosynthetic electron transport chain (ETC) and therefore the conversion of light energy to organic carbon products [9–11].

Approaches currently used to measure phytoplankton primary production quantify rates at different points of the photosynthetic process (evolution of O_2, assimilation of CO_2, electron transport in photosystem II). These various rates can be decoupled in response to changes in environmental conditions or phytoplankton taxonomy [12]. For this reason, it is likely that iron limitation will affect the conversion factors between these various productivity metrics. Phytoplankton CO_2-assimilation can be measured directly using the radioisotope tracer ^{14}C [13,14]. This technique has been widely applied in biological oceanography over the past 60 years, despite a number of well-known limitations (e.g. low spatial and temporal resolution, high cost and labour intensity, bottle artifacts due to exclusion of grazers and contamination, requirement for radio-isotopes, ambiguity of whether net or gross production is measured [14–18]). In recent years, bio-optical approaches have emerged as an attractive alternative to overcome these limitations. Chlorophyll a fluorescence (ChlF) yields, measured by Pump and Probe, FRR, or PAM fluorometry, can be used to estimate rates of linear electron transport (i.e. rates of charge separation) in photosystem II (ETR_{RCII}) [19–23], thus providing a measure of gross photosynthesis. Being non-intrusive, instantaneous and relatively inexpensive, these approaches can be used to examine phytoplankton photophysiology at unmatched spatial and temporal resolution, and improve the coverage of productivity estimates over vast oceanic domains.

Despite significant potential, active ChlF approaches are currently not widely applied to monitor rates of phytoplankton primary productivity. This is due, in part, to uncertainty in the conversion of ETR_{RCII} to ecologically relevant rates of CO_2-assimilation [12, 24]. Numerous studies conducted over the past decades have collectively shown that the conversion factor linking ETR_{RCII} to CO_2-assimilation in phytoplankton is not constant, but changes in response to taxonomy and environmental conditions [12, 20, 24–53]. On the physiological level, ETR_{RCII} and CO_2-assimilation can be uncoupled by a number of energy-allocation processes that evolved to maximize photosynthetic efficiency while preventing photodamage. Marine phytoplankton evolved an exceptional photosynthetic plasticity to achieve this balance under low nutrient and fluctuating light conditions. A number of recent studies have examined this fine-tuning of electron transport and energy allocation within the phytoplankton photosynthetic apparatus, providing mechanistic insight into the processes decoupling CO_2-assimilation and photosynthetic electron transport (e.g. [54–63]).

In this study, we examine the interacting effects of iron levels and instantaneous light availability on the coupling of ETR_{RCII} and CO_2-assimilation in marine phytoplankton. We derived rates of ETR_{RCII} normalized to PSII reaction center content (mol e$^-$ mol RCII^{-1} s^{-1}), resulting in a conversion factor consisting of two parameters: the amount of chlorophyll a (chl a) functionally connected to each RCII ($1/n_{PSII}$, mol chla^{-1} mol RCII^{-1}), and the electron requirement for carbon fixation ($\Phi_{e:C}$, mol e$^-$ mol C). Working with natural phytoplankton assemblages in the Northeast subarctic Pacific, and mono-specific phytoplankton cultures in the laboratory, we conducted simultaneous measurements of FRRF-derived ETR_{RCII} and ^{14}C-based CO_2-assimilation over a range of irradiances (PvsE curves) under high and low iron conditions. Our results demonstrate significant and interactive effects of irradiance and iron availability on the coupling of ETR_{RCII} and CO_2-assimilation, with an increase in the conversion factor $\Phi_{e:C}/n_{PSII}$

under excess light and low iron conditions. From a photophysiological point of view, increased decoupling appeared to be caused by the effects of increased excitation pressure on the photosynthetic ETC, resulting in a strong correlation between the derived conversion factor and the expression of non-photochemical quenching (NPQ) in the antennae of PSII. This correlation can, in turn, be used to derive rates of carbon-based productivity from FRRF data, without the need for any additional measurements.

Methods

In this study, we utilized three separate datasets. First, we examined the coupling of ETR_{RCII} and CO_2-assimilation in a mixed phytoplankton assemblage during a 6 day ship-board iron addition experiment in iron-limited waters of the subarctic Pacific (Fig 1). Secondly, we conducted experiments with two mono-specific phytoplankton cultures grown under controlled light and iron conditions in the laboratory. These experiments were conducted to examine the physiological effects of iron and light on the conversion factor $\Phi_{e:C}/n_{PSII}$, in the absence of potentially confounding taxonomic shifts. Finally, we applied the results obtained from the iron addition experiment to derive a conversion factor predicting rates of CO_2-assimilation along a coastal to open ocean transect in the NE subarctic Pacific (Line-P, https://www.waterproperties.ca/linep/) (Fig 1). All fieldwork for this project was conducted under the authorization and permits of Fisheries and Oceans Canada.

Iron addition experiment

All fieldwork was conducted on board the *CCGS John P. Tully* in August—September 2013. A 6 day iron addition experiment was initiated at P20 (49°34 N, 138°40 W) (Fig 1), located in iron-limited HNLC waters. Water was collected before dawn from 7 m depth using a trace metal clean pumping system and an on-deck class 100 laminar flow hood (cf. [64]). In order to eliminate macro-zooplankton, the water was pre-filtered through acid washed 200 μm Nitex mesh. Six trace metal-cleaned 10 L cubitainers were rinsed and filled in random order. Triplicate iron-addition treatments were amended with 1 nM Fe (ammonium iron (II) sulfate hexahydrate $((NH_4)_2Fe(SO_4)_2\cdot6H_2O)$, dissolved in 0.05M HCl), while triplicate controls were left unamended. Cubitainers were kept in on-deck incubators continuously supplied with seawater pumped from 5 m depth. Light intensity was adjusted to ~ 50% of full sunlight with neutral density screening and irradiance was continuously logged using a LI-1000 radiation sensor (LI-COR, USA), located 2 m above the incubator. This level of light reduction was chosen to avoid exposing the phytoplankton to irradiances higher than in situ values. On days 1, 3 and 5 at exactly 2 hours after local sunrise, 500 mL of water were sub-sampled from each cubitainer using trace metal clean techniques. Sub-samples were analyzed for total chlorophyll *a* concentration ([chl *a*]), photophysiological parameters and rate measurements as outlined below. On the last day of the experiment, additional samples were collected for pigment analysis by high pressure liquid chromatography (HPLC), and the determination of absorption spectra using the quantitative filter technique (QFT) [65].

Laboratory culturing

The oceanic centric diatom *Thalassiosira oceanica* (CCMP isolate 1003, Sargasso Sea) and the oceanic prymnesiophyte *Chrysochromulina polylepis* (NEPCC isolate 242, NE subarctic Pacific) were grown under iron-replete and iron-limiting conditions. We chose these two species as representative eukaryotic open ocean species, common in the region of our field study [66,67]. Iron-limited growth conditions were chosen to achieve an approx. 50% reduction in growth rate. Both species were cultured in 28 mL acid-cleaned polycarbonate tubes using the
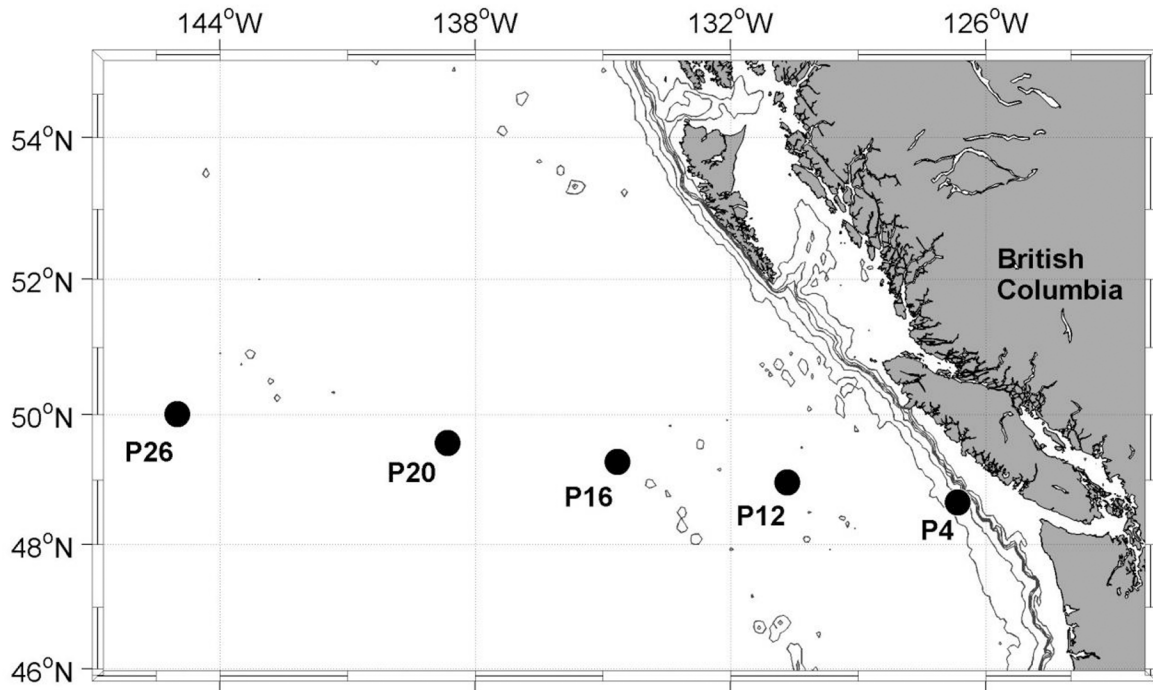
Fig 1. Map of sampling stations along the Line-P transect in the NE subarctic Pacific. The iron addition experiment was initiated at station P20, located in iron-limited high nutrient low chlorophyll (HNLC) waters. Sampling depths at other stations along the transect were: 30 m at P4; 5 m, 25 m and 40 m at P12, P16, P20 and P26.

artificial seawater medium AQUIL [68], prepared as described by Maldonado et al. [69]. All cultures were kept at 19°C in continuous, sub-saturating light (ca. 40 μmol quanta m^{-2} s^{-1}). Growth was monitored by daily measurements of in vivo chl *a* fluorescence using a Turner 10-AU Fluorometer, and cultures were kept in exponential growth phase using semi-continuous batch culturing [70]. Cultures were considered acclimated when growth rates during ca. 40 cell divisions (five successive transfers), varied by <15% [70]. Acclimated, exponentially growing cells were used to inoculate triplicate 200 mL cultures. These 200 mL cultures were subsampled several times for FRRF measurements (see below), which demonstrated that cells maintained steady-state photophysiology throughout the sampling phase. During early to mid-exponential phase, each replicate culture was sampled for duplicate ETR$_{RCII}$-P*v*E curves, duplicate ^{14}C-P*v*E curves and triplicate [chl *a*] samples. Sterile, trace metal clean techniques were used at all times.

Station sampling

In addition to the iron addition experiment, seawater samples were collected at five hydrographic stations (P4, P12, P16, P20, and P26) spanning a coastal to open ocean transect in the NE subarctic Pacific (Fig 1). Collection of water column hydrographic profiles was performed with a CTD (SeaBird Electronics, model 911 plus) equipped with a dissolved oxygen sensor (SBE 43), fluorometer (Seapoint), and an underwater photosynthetically active radiation (PAR) sensor (Biospherical QSP-400). At each of the stations, water was collected from Niskin bottles at three depths exactly two hours after local sunrise and processed immediately for rate measurements, photophysiological parameters, and [chl *a*] as described below.

[chl *a*]

For the 3 sets of experiments outlined above, samples for [chl *a*] were filtered onto pre-combusted 25 mm glass fiber filters (GF/F) using low vacuum pressure (<5 mm Hg) and analyzed following the method of Welschmeyer [71]. In the field, triplicate 100–300 mL samples were filtered and stored at -20°C until analysis within three weeks of collection. In the laboratory, triplicate culture samples (10 mL, 20 mL and 30 mL) were collected and analyzed immediately. Each sample was analyzed in duplicate.

Carbon assimilation

For both laboratory and field work, rates of carbon assimilation were measured as small volume P*vs*E curves in a custom built photosynthetron [72]. In the field, 300 mL of water were spiked with 150 µCi NaH^{14}CO$_3$ (final concentration 0.5 µCi mL^{-1}, 52.5 mCi mL^{-1} specific activity) (Perkin-Elmer) immediately after sampling. Spiked samples were mixed gently but thoroughly, aliquoted into 20 ml glass scintillation vials and placed into the photosynthetron. Temperature was kept within 1°C of in situ temperature by circulating water from a water-bath through an aluminum cooling jacket (the offset from in situ temperature was larger for station samples because samples from different depth had to be incubated simultaneously). Light was provided by high power light emitting diodes (LEDs) located under each scintillation vial. Each P*vs*E curve consisted of 11 light levels spanning intensities from 3 to 600 µmol quanta m^{-2} s^{-1}. Actual light intensities were measured before and after each experiment using a 4π quantum sensor (QSL-2100, Biospherical Instruments) immersed in water inside a scintillation vial. Incubations lasted for 3–4 hours and were ended by gentle filtration onto 25 mm GF/F filters. Filters were pre-combusted to reduce nominal pore size to approx. 0.4 µm. For each curve, three time-zero samples were taken by filtering 20 mL immediately after spiking. The total ^{14}C activity added was determined from three 1 mL aliquots of the spiked sample added to 1 mL 1 M NaOH. All work was done under low light and filters were stored in scintillation vials at -20°C until processing within 1 month of the experiment. During laboratory processing, 500 µL of 3 M HCl was added to each filter and vials were left to degas for >24 hours to eliminate any inorganic ^{14}C remaining in the samples. Ten mL of scintillation cocktail (Scintisafe plus, Fisher) were added to each vial, and vials were then vortexed and left to stand in the dark for >12 hours before analysis on a liquid scintillation counter (Beckman). Disintegrations per minute (DPM) were derived from scintillation counts using a quench curve prepared from commercial ^{14}C standards (Perkin-Elmer). DPM were converted to units of carbon biomass following Knap et al. [73].

The ^{14}C protocol used for laboratory cultures was the same as outlined above with the following exceptions. We spiked 80 mL of exponentially growing culture with 40 µCi NaH^{14}CO$_3$ and 3 mL aliquots were incubated in the photosynthetron for 30 minutes. Duplicate curves were measured for each sample. The incubation was terminated by adding 1 mL of 1 M HCl to each vial and samples were dried completely, omitting the filtration step. After drying, salts were re-suspended in 1 mL MilliQ water. For both laboratory and field measurements ^{14}C-P*vs*E curves were fit following Webb et al. [74], as described below.

Chl *a* fluorescence parameters and ETR$_{RCII}$

A bench-top FRRF instrument (Soliense Inc.) was used for all active ChlF measurements. In the field, opaque bottles were used for sub-sampling from the rosette or iron addition experiment, and light in the laboratory was kept low at all times to allow oxidation of the ETC and relaxation of NPQ. For all measurements, background fluorescence blanks were prepared by very gently filtering a small amount of sample through a pre-combusted GF/F. Single turnover

(ST) flash protocols consisted of 100 flashlets with 1.0 μs length and 2.5 μs interval (46200 μmol quanta m^{-2} s^{-1} peak power intensity, resulting in a ST flash length of 250 μs, providing ~5–10 quanta per RCII). The excitation power was selected at the beginning of the cruise to saturate the observed fluorescence transients within the first half of the ST excitation protocol. Our experience indicates that this approach offers the best signal-to-noise ratio in the recovered parameters, while accommodating significant variations in the photosynthetic properties of the local phytoplankton populations along the cruise track, without re-adjusting of the excitation protocol. Excitation power was provided by an array of eight LEDs at four wavelengths centered on 445 nm, 470 nm, 505 nm, and 530 nm (equal intensity at each wavelength; see S1 Fig for more information on the spectral distribution). We measured steady state light curves (SSLC), where each sample was exposed to 10 actinic 'background' irradiances ranging from 0 to 1000 μmol quanta m^{-2} s^{-1}, also provided at four wavelengths (S1 Fig). The relatively long duration of the SSLCs in this study could create some potential for the settling of cells which could influence the ChlF yield. However, our sampling region is known to be dominated by small cells [66], which should have a slow settling rate. Equally, the laboratory isolates used during this study stay in suspension for many hours, and it is thus unlikely that rapid settling of cells drastically altered our results.

All ChlF yields and parameters described below were derived by an iterative non-linear fitting procedure, applying the four parameter biophysical model of Kolber et al. [21] to a mean of 20 consecutive ST flashes using custom software (Z. Kolber). This software accounts for a formation of fluorescence quenching, most likely due to formation of a P680 triplet, which reduces the maximum fluorescence yield attainable during the ST flash by 3–6%. Throughout the SSLC, ST flashes were applied continuously (at 1 s interval), while the length of each light step was optimized to allow all derived parameters to reach steady state (ca. 5 min). ChlF yields and parameters corresponding to each light level were obtained from the mean of the last three acquisitions at each light level. In this way, we derived the fluorescence yields F_o and F_m (in dark regulated state) as well as F' and F_m' (in the light regulated state for each light level of the SSLC). F_o' was calculated as $F_o' = F_o/(F_v/F_m + F_o/F_m')$ [75]. Even though this derivation has become widely accepted in the literature, we caution here that it might not hold for values derived under high background irradiance (see [76]) and varying stress levels experienced by natural phytoplankton assemblages.

Five fluorescence signals, F_o, F_m, F', F_m' and F_o' were used to calculate ChlF parameters, following Roháček [77]. In the dark-regulated state, we derived the commonly used F_v/F_m ratio as $F_v/F_m = (F_m-F_o)/F_m$ [78]. For each light level of the SSLC protocol we have calculated the following ChlF parameters: (1) The photochemical quenching of variable fluorescence, $F_q'/F_v' = (F_m'-F')/(F_m'-F_o')$, which quantifies the fraction of functional RCII in the open state (i.e. primary quinone acceptor Q_A in the oxidized state) [79]. (2) The maximum quantum yield of PSII photochemistry, $F_v'/F_m' = (F_m'-F_o')/F_m'$, which can be used to quantify the extent to which photochemistry in PSII is limited by competition with thermal decay of excitation energy [75]. (3) The overall quantum efficiency of photochemical energy conversion in PSII at a given light intensity (note that numerous definitions for this parameter exist in the literature), $F_q'/F_m' = (F_m'-F')/F_m' = \Phi_{PSII}'$ (the product of F_q'/F_v' and F_v'/F_m' [19]). Furthermore, the functional absorption cross section of PSII, σ_{PSII} ($Å^2$ $RCII^{-1}$), was derived from the rate of closure of RCII in the dark-regulated and at each light-regulated state [20,21]. The connectivity parameter, ρ, was also calculated, but not used in our analysis.

Rates of charge separation (i.e. ETR_{RCII}) in functional RCII (mol e^- mol $RCII^{-1}$ s^{-1}) were estimated as the product of incident irradiance (E), the fraction of irradiance absorbed by PSII (σ_{PSII}) and the efficiency with which charge separation occurs in RCII. We calculated ETR_{RCII}

as

$$\text{ETR}_{\text{RCII}} = \text{E} * \sigma_{\text{PSII}}{}' * \frac{\text{F}_q{}'}{\text{F}_v{}'} * 6.022 * 10^{-3} \qquad (1)$$

where E (μmol quanta m^{-2} s^{-1}) is the actinic irradiance at each light level, $\sigma_{\text{PSII}}{}'$ (Å^2 RCII^{-1}) is the functional absorption cross section at E and $\text{F}_q{}'/\text{F}_v{}'$ is the photochemical capacity of PSII at E. The number 6.022 x 10^{-3} converts μmol quanta to quanta and Å^2 to m^2. Because of potential systematic errors in the calculation of $\text{F}_o{}'$, we also calculated ETR$_{\text{RCII}}$ as

$$\text{ETR}_{\text{RCII}} = \text{E} * \sigma_{\text{PSII}} * \frac{(\text{F}_q{}'/\text{F}_m{}')}{(\text{F}_v/\text{F}_m)} * 6.022 * 10^{-3} \qquad (2)$$

which does not require the knowledge of $\text{F}_o{}'$. Both calculations are equivalent, assuming that non-photochemical quenching processes affecting ChlF can be adequately accounted for in either the absorption term (Eq 1) and the efficiency term (Eq 2). While Eq 2 does not require $\text{F}_o{}'$ (which was not measured directly) or $\sigma_{\text{PSII}}{}'$ (which is difficult to derive at high irradiances), it does rely on parameters measured in the fully dark-regulated state, which can be difficult to achieve in field assemblages. For all ETR$_{\text{RCII}}$ calculated during our iron addition experiment (n = 345) the difference between values calculated in both ways ranged from 0.5 to 21% with a mean coefficient of variance of 5.5%. Both approaches thus provided similar results in the analysis of our data, and the differences observed were not systematically related to the treatment (high *vs* low Fe).

Non-photochemical quenching (NPQ) at each light level was estimated as the normalized Stern-Volmer quenching coefficient, defined as NPQ$_{\text{NSV}}$ = ($\text{F}_m{}'/\text{F}_v{}'$)-1 = $\text{F}_o{}'/\text{F}_v{}'$ [65]. Quantification of NPQ using NPQ$_{\text{NSV}}$ instead of the more commonly used Stern-Volmer coefficient of quenching, defined as NPQ$_{\text{SV}}$ = (F_m-$\text{F}_m{}'$)/F_m [80], is appropriate for our data-set, as it resolves differences between NPQ present in the dark-regulated state.

P*vs*E curves

Measurements of CO_2-assimilation and ETR$_{\text{RCII}}$ were plotted against irradiance, and the exponential model of Webb et al. [74] was fit to the data using a non-linear least squares regression procedure in Matlab. For the CO_2-assimilation data, an intercept parameter was added to force the regression through the origin and provide a good fit in the linear part of the P*vs*E curve [28,81]. For both rates of productivity, we derived the light saturated maximum rate P$_{\text{max}}$ and the light utilization efficiency α. When photoinhibition was observed at high irradiances, the data-points were excluded from the fitting procedure.

Derivation of conversion factor

Because we derived ETR$_{\text{RCII}}$ in units of mol e$^-$ mol RCII^{-1} s^{-1} and CO_2-assimilation in units of mol C mol chl a^{-1} s^{-1}, the conversion factor between the two rates accounts for changes in chl a functionally associated with each RCII (1/n$_{\text{PSII}}$, mol chl a mol RCII^{-1}) and the number of charge separations in RCII needed per CO_2-assimilated into organic carbon products ($\Phi_{\text{e:C}}$, mol e$^-$ mol C^{-1}).

$$\frac{\textbf{ETR}_{\text{RCII}}(\text{mol e}^- \text{ mol RCII}^{-1} \text{ s}^{-1})}{\textbf{CO}_2 \textbf{ assimilation}(\text{mol C mol chl } a^{-1} \text{ s}^{-1})} = \Phi_{\text{e:C}} \left(\frac{\text{mol e}^-}{\text{mol C}} \right) * \frac{\textbf{1}}{\textbf{n}_{\textbf{PSII}}} \left(\frac{\text{mol chl } a}{\text{mol RCII}} \right) \quad (3)$$

In this approach, we attribute the observed decoupling between ETR$_{\text{RCII}}$ and CO_2-assimilation to changes in both, 1/n$_{\text{PSII}}$ and $\Phi_{\text{e:C}}$. We recognize that combining $\Phi_{\text{e:C}}$ and 1/n$_{\text{PSII}}$ into

one conversion factor obscures the mechanistic underlying of the observed decoupling. Nevertheless, as we will show, our approach has the potential to provide FRRF-derived estimates of phytoplankton primary productivity in carbon units without the need for many of the auxiliary measurements and inherent assumptions used in previous studies.

The value of $1/n_{PSII}$ is known to change significantly as a function of taxonomy [22], light [22,82], macro-nutrients [83], and iron availability [84–90]. Therefore we could not assume a constant value for $1/n_{PSII}$, as has been done in most previous studies [24]. Although $1/n_{PSII}$ can be directly measured from oxygen flash yield experiments (e.g. [91–93]), the approach is labour-intensive and not practical for routine field sampling. A new approach to derive [RCII] directly from FRRF measurements has been developed [94,95], but not implemented in our study because the inherent assumption that the ratio of rate constants of photochemistry and fluorescence (k_p/k_f) is confined to a narrow range, does not hold under varying levels of iron limitation [62,87,94].

Having established a relationship between light intensity and rates of CO_2-assimilation and ETR_{RCII} for each sample, we were able to model the light dependency of the conversion factor $\Phi_{e:C}/n_{PSII}$. This approach allowed us to observe how the coupling of ETR_{RCII} and CO_2-assimilation is modulated by incident irradiance, and how, in turn, iron limitation influences the light-dependent response. Additionally, we used α and P_{max} of each rate to derive the conversion factor under sub-saturating and saturating light conditions, respectively.

Results

Effect of iron addition on phytoplankton community composition, photophysiology, ETR_{RCII} and CO_2-assimilation in the NE subarctic Pacific

Phytoplankton assemblages at station P20 in the NE subarctic Pacific (Fig 1) responded strongly to iron addition in a ship-board incubation experiment (Fig 2). Six days after iron addition, [chl a] increased by an order of magnitude, whereas the control (i.e. no iron addition) showed only a small increase in [chl a]. This result confirms that the initial phytoplankton assemblage was iron-limited (Fig 2A), and that we were able to carry out the manipulation experiment without significant contamination of the control bottles. The slight increase in [chl a] in the control treatments is likely attributable to a decrease in grazing pressure and to changes in the light environment (i.e. lower and less fluctuating light). Iron addition also significantly affected phytoplankton photophysiology, as demonstrated by rapid changes in the parameters σ_{PSII} and F_v/F_m derived in the dark-regulated state (Fig 2B and 2C). F_v/F_m initially increased in both treatments, but then remained low in the control while continuing to increase in the iron addition treatment (Fig 2B). While the functional absorption cross-section of PSII, σ_{PSII} ($Å^2$ $RCII^{-1}$), remained high and relatively constant in the iron-limited control, it declined rapidly after iron addition, and remained ~25% lower than that of the initial phytoplankton assemblage (Fig 2C). The observed changes in F_v/F_m and σ_{PSII} may have resulted from both, photophysiological responses and from changes in species composition. CHEMTAX analysis of pigments sampled on day 6 of the experiment showed that the addition of iron changed the taxonomic composition of the phytoplankton assemblage (S2 Fig). Most prominently, the abundance of chlorophytes decreased from 7% to 1%, prymnesiophytes decreased from 55% to 22%, pelagophytes increased from 17% to 39%, and diatoms increased from 1% to 16% in iron amended bottles. A similar response has been observed in previous iron addition experiments conducted in this region [96].

We measured PvsE curves of short-term CO_2-assimilation and ETR_{RCII} five times during the iron addition experiment (Fig 3). Both rates show the expected light dependency, and were affected by iron addition. However, the response to iron addition differed for CO_2-assimilation
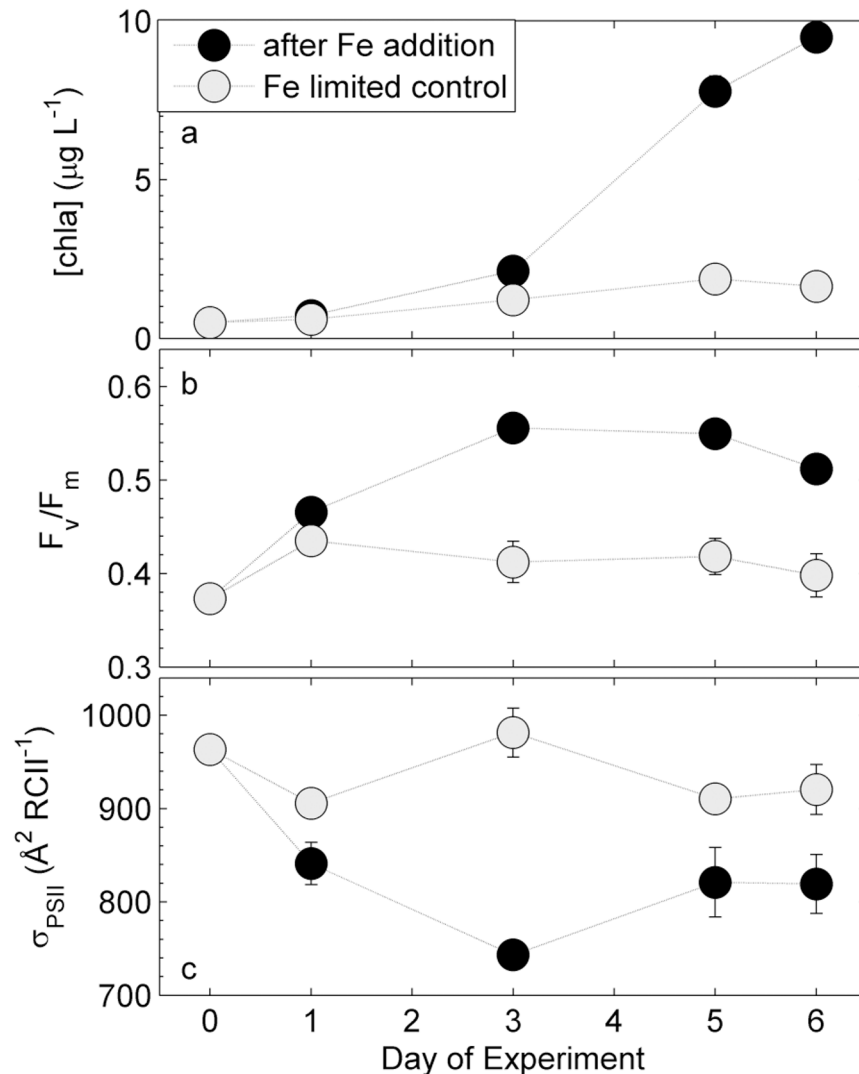
Fig 2. Response of chl *a* biomass and photophysiology during the on-board iron addition experiment.
Shown are changes in (a) [chl *a*], (b) F_v/F_m, and (c) σ_{PSII}. Error bars represent standard errors from three biological replicates and are sometimes smaller than the symbol.

and ETR_{RCII}. Chlorophyll *a*-normalized CO_2-assimilation showed a small, though not statistically significant, increase after iron addition (Fig 3A–3E). The observed increase in the chl *a*-normalized rate was small, because cellular chl *a* content increased in parallel with CO_2-assimilation (under all nutrient limitations, cellular chl *a* in phytoplankton is drastically reduced, a condition referred to as chlorosis, e.g. [97]). The strong effect of iron addition on CO_2-assimilation can be seen more clearly when rates are normalized to volume. Indeed, volume-normalized CO_2-assimilation rates increased more than 8-fold after iron addition in this experiment (S3 Fig). In contrast to rates of CO_2-assimilation, ETR_{RCII} decreased significantly after iron addition, when compared to the iron-limited control treatment (Fig 3F–3J).

The response of CO_2-assimilation and ETR_{RCII} to iron addition is further visualized in Fig 4, which shows changes in light-limited slopes (α) and light saturated rates (P_{max}), as well as the derived conversion factor $\Phi_{e:C}/n_{PSII}$ for α and P_{max}, throughout the experiment. Values for α and P_{max} were derived from the ^{14}C-based and FRRF-based P*vs*E curves shown in Fig 3. No
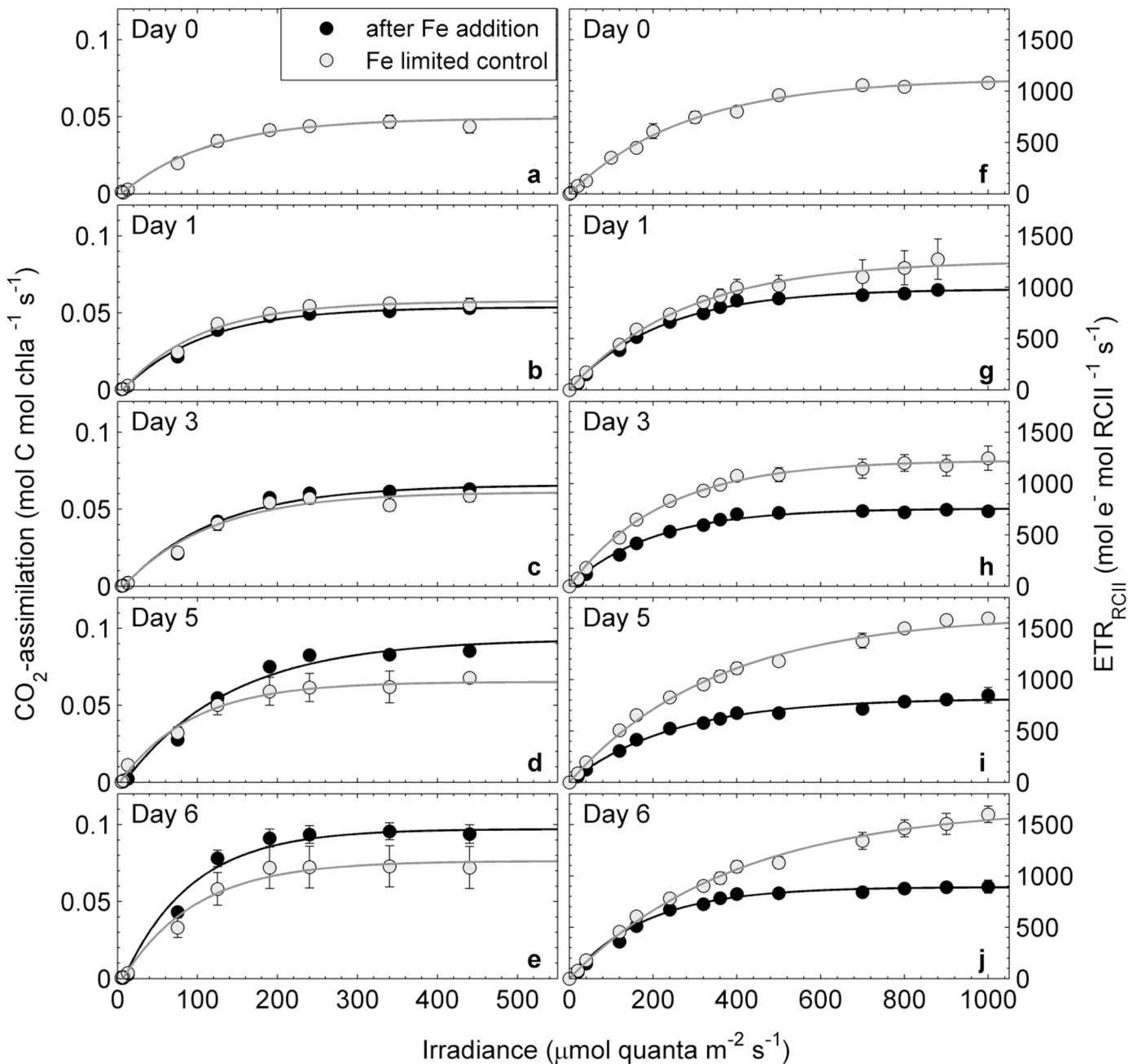
Fig 3. Response of rates of CO$_2$-assimilation (mol C mol chl a^{-1} s^{-1}) and ETR$_{RCII}$ (mol e$^-$ mol RCII^{-1} s^{-1}) during the iron addition experiment. Both rates were measured as a function of irradiance, and PvsE curves were fit with the exponential model of Webb et al. [74]. Shown are mean values from three biological replicates where error bars represent standard error of mean and are sometimes smaller than symbols.

doi:10.1371/journal.pone.0133235.g003

statistically significant change in values of α could be determined for either chl a-normalized CO$_2$-assimilation, ETR$_{RCII}$ or $\Phi_{e:C}/n_{PSII}$ (p-value > 0.05). Similarly, the P$_{max}$ for chl a-normalized CO$_2$-assimilation remained relatively constant in the control, and did not show a statistically significant increase after iron addition (p-value > 0.05) (Fig 4D). In contrast, there was a significant (p-value < 0.05) decrease in P$_{max}$ for ETR$_{RCII}$ following iron-addition, as compared to the control treatments, which exhibited a small increase in this variable over the course of
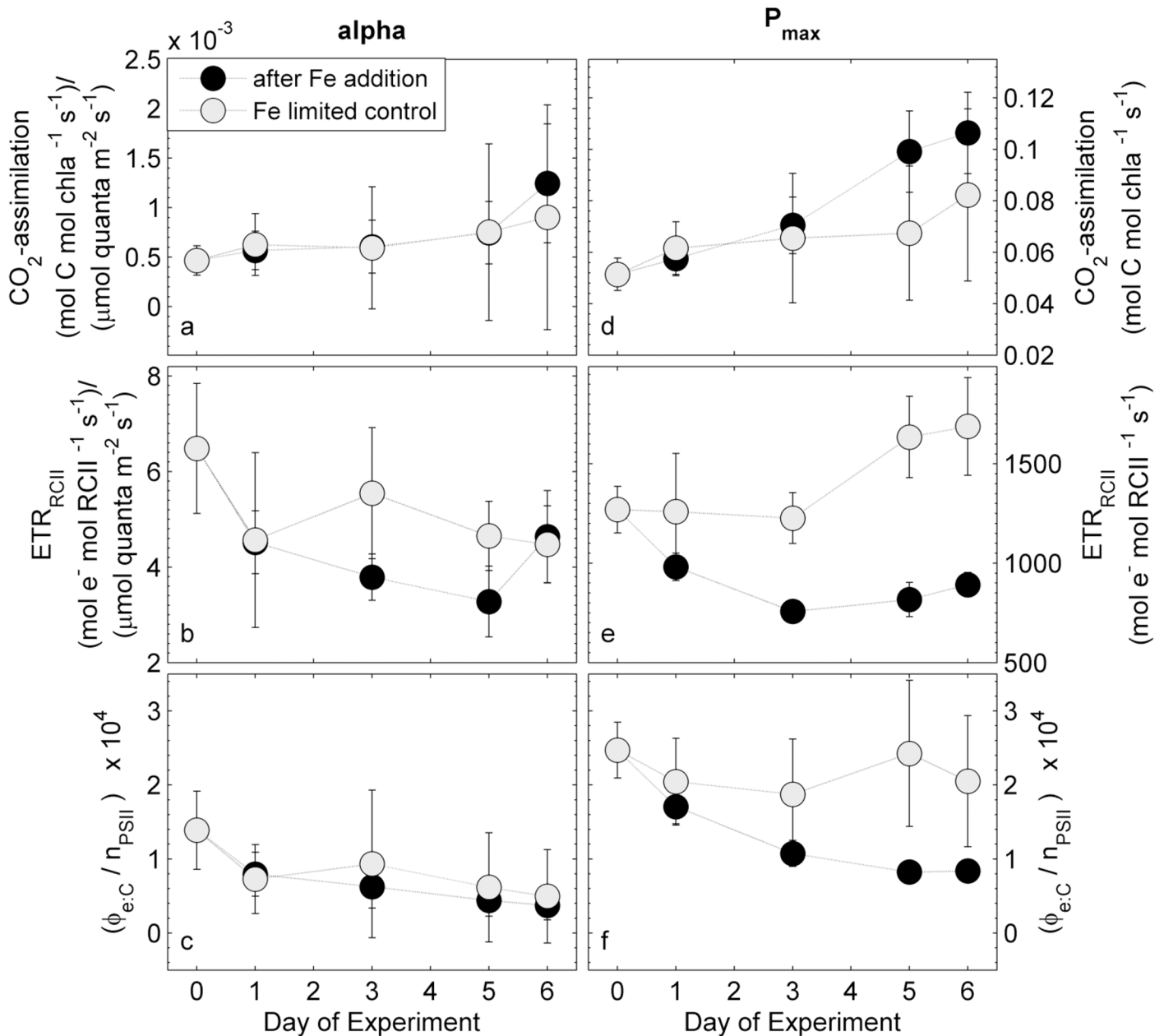
Fig 4. Time-course of α (a-c) and P$_{max}$ (d-f) of CO$_2$-assimilation, ETR$_{RCII}$ and the derived conversion factor Φ$_{e:C}$/n$_{PSII}$ during the iron addition experiment. The conversion factor Φ$_{e:C}$/n$_{PSII}$ under light limiting conditions is derived from values in (a) and (b). Similarly, the conversion factor Φ$_{e:C}$/n$_{PSII}$ at light saturation is derived from the values in (d) and (e). The error in (a), (b), (c), and (d) is the 95% confidence interval of the parameter derived from the fit to data from three biological replicates, and the error in (c) and (f) is the propagated error from (a)/(b) and (d)/(e), respectively.

the experiment (Fig 4E). The observed changes in the P$_{max}$ for CO$_2$-assimilation and ETR$_{RCII}$, resulted in a decrease in Φ$_{e:C}$/n$_{PSII}$ in the iron addition treatment compared to the relatively constant value observed in the iron-limited control (Fig 4F). This difference was statistically significant for the last 2 days of the experiment (p-value < 0.05). When compared to the initial value on day 0 of the incubation, the conversion factor Φ$_{e:C}$/n$_{PSII}$ for P$_{max}$ decreased by 66% after iron addition, and by 16% in the iron-limited control (Fig 4F). These results indicate that

the iron-dependent changes in $\Phi_{e:C}/n_{PSII}$ are most readily apparent under high irradiance conditions where photosynthesis is light-saturated.

To better explain the iron-dependent decrease in ETR_{RCII} and $\Phi_{e:C}/n_{PSII}$ observed in our data, we examined changes in additional FRRF-derived ChlF parameters, measured on day 3 after iron addition. We choose day 3 for the in-depth analysis of our data, but trends observed on this day were representative of those observed throughout the experiment. The parameter F_q'/F_v' represents the efficiency of charge separation in functional RCII (Fig 5A). It is an estimate of the fraction of open RCII (i.e. Q_A oxidized) at any given light level, and therefore always equals one at zero irradiance. On day 3 after iron addition, we observed higher F_q'/F_v' for the iron-limited control at all irradiance levels (Fig 5A), indicating a greater fraction of open reaction centers. The parameter F_v'/F_m', the efficiency of excitation energy capture by the
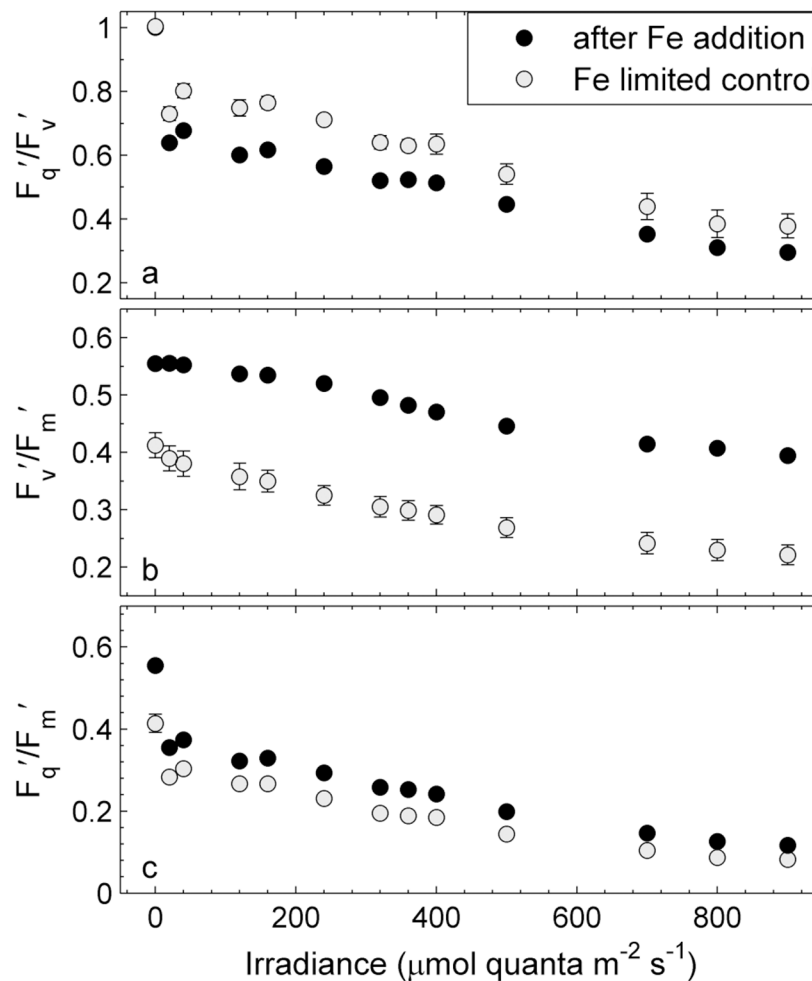

Fig 5. Light dependency of ChlF-derived parameters from FRRF measurements on day three after iron addition and in the iron-limited control treatment. The parameter F_q'/F_v' (a) represents the efficiency of charge separation in functional RCII and is an estimate of the fraction of open RCII (i.e. Q_A oxidized) at any given light level. The parameter F_v'/F_m' (b) represents the efficiency of excitation energy capture by the fraction of open RCII and can be used to quantify the extent to which non-photochemical quenching in the PSII antenna competes with photochemistry for excitation energy. The parameter F_q'/F_m' (c) represents the overall quantum efficiency of photochemical energy conversion in PSII (Φ'_{PSII}). See text for a full description of these parameters and their interpretation. Error bars represent standard errors from three biological replicates and are often smaller than symbols.

doi:10.1371/journal.pone.0133235.g005

fraction of open RCIIs [19], can be used to quantify the extent to which photochemistry in RCII is limited by thermal energy dissipation in the antenna [75]. This parameter was significantly reduced in the iron-limited control relative to the iron addition treatment (Fig 5B), indicating that the efficiency of excitation energy transfer in the light-harvesting antenna was comprised. The overall efficiency of charge separation per quantum absorbed in PSII (F_q'/F_m') is the product of F_q'/F_v' and F_v'/F_m' [19,77]. On day 3, at all light levels, F_q'/F_m' was higher in the iron addition treatment than in the iron-limited control (Fig 5C).

We used our PvsE measurements of CO_2-assimilation and ETR_{RCII} to examine the light-dependent response of the conversion factor $\Phi_{e:C}/n_{PSII}$. Our results (Fig 6) show that $\Phi_{e:C}/n_{PSII}$ increased with increasing irradiance, regardless of iron treatment and day of the experiment (Fig 6A–6E). However, this light-dependent increase was much more pronounced in the iron-limited control treatment. It is important to note that the magnitude and light-dependency of $\Phi_{e:C}/n_{PSII}$ in the iron-limited control treatment changed over the course of the experiment relative to the initial sample (Fig 6A). This shift in $\Phi_{e:C}/n_{PSII}$ in the absence of iron addition likely reflects changes in light quality and quantity in the incubation bottles relative to the ambient water column.

Also shown in Fig 6 is the light and iron dependency of NPQ_{NSV}, estimated as F_o'/F_v'. This parameter showed a light and iron-dependent response that was remarkably similar to $\Phi_{e:C}/n_{PSII}$, with values increasing with increasing light, regardless of treatment and day of the experiment, and decreasing in response to iron addition (Fig 6F–6J). The NPQ_{NSV} values measured in our initial sample (Fig 6F) were higher than those measured in either control or iron addition treatments during the following days. We attribute this effect to a more stable light environment in the incubation bottles, relative to in situ irradiance levels.

Given the similar light and iron-dependent responses of $\Phi_{e:C}/n_{PSII}$ and NPQ_{NSV}, we sought to examine the relationship between these two variables. In order to do so, however, it was necessary to derive NPQ_{NSV} and $\Phi_{e:C}/n_{PSII}$ values at a standard set of light levels, matching those of the FRRF derived ETR_{RCII}-PvsE curves. For each sample, ETR_{RCII}-PvsE curves consisted of 14 light levels spanning from 0 to 1000 µmol quanta m^{-2} s^{-1}. These light levels did not exactly match those used for the CO_2-assimilation experiments. We thus used the PvsE curve fits of our ^{14}C data to derive the CO_2-assimilation values at light levels matching those of the ETR_{RCII}-PvsE curves. In this way, we were able to compile a dataset of 298 paired values for NPQ_{NSV} and $\Phi_{e:C}/n_{PSII}$, derived from 27 sets of ETR_{RCII} and ^{14}C PvsE curves during the iron addition experiment. Plotting these $\Phi_{e:C}/n_{PSII}$ values against the corresponding NPQ_{NSV} reveals a strong and statistically significant correlation ($R^2 = 0.70$, p-value < 0.0001, for quadratic fit) (Fig 7).

Effects of iron limitation on photophysiology and rates of ETR_{RCII} and CO_2-assimilation in mono-specific phytoplankton cultures

Using methods analogous to those applied to mixed phytoplankton assemblages in the NE subarctic Pacific; we measured PvsE curves of CO_2-assimilation and ETR_{RCII} in mono-specific laboratory cultures of two open ocean phytoplankton species. The results, summarized in Table 1, show similar trends as observed in our field data. Steady-state growth rates (μ, d^{-1}) in the low iron cultures were 68% and 49% of iron-replete growth rates in *T. oceanica* and *C. polylepis*, respectively (Table 1). For both species, F_v/F_m in iron-limited cultures was reduced (by 32% and 20% in *T. oceanica* and *C. polylepis*, respectively). In iron-limited *T. oceanica*, σ_{PSII} increased by 15%, while it increased by 5% in *C. polylepis*. The iron dependent changes in μ, F_v/F_m and σ_{PSII} was statistically significant in both species (one tailed p-value < 0.0001 and < 0.01 for *T. oceanica* and *C. polylepis*, respectively). Chlorophyll *a*-normalized CO_2-assimilation at P_{max} remained relatively constant in both species (p-value > 0.05). In contrast,
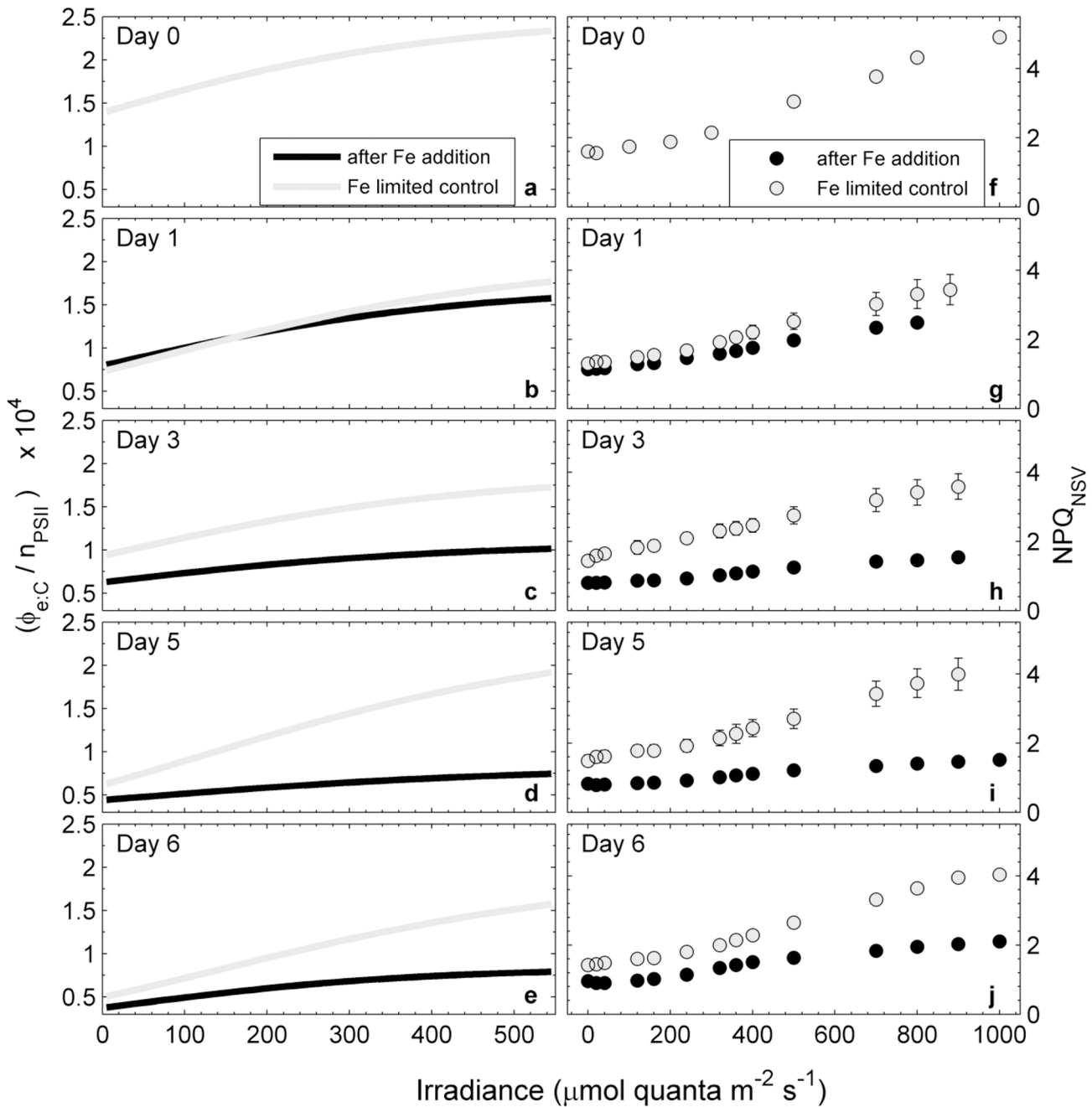
Fig 6. Changes in the light dependency of the conversion factor $\Phi_{e:C}/n_{PSII}$ (a-e) and NPQ_{NSV} (f-j) over the course of the iron addition experiment.
Units of in $\Phi_{e:C}/n_{PSII}$ are (mol e- mol C) / (mol chl a mol RCII^{-1}). The curves were derived by dividing corresponding values of ETR_{RCII} and CO_2-assimilation from the PvsE curves presented in [Fig 3](). NPQ was estimated as the normalized Stern-Volmer quenching coefficient $NPQ_{NSV} = F_o'/F_v'$ and is unitless [65]. Error bars are the standard error from three biological replicates and often smaller than symbols.

doi:10.1371/journal.pone.0133235.g006

we observed a 90% increase in ETR_{RCII} at P_{max} in *T. oceanica* under iron-limited growth conditions. *C. polylepis* also exhibited an increase in ETR_{RCII} at P_{max} under iron-limited conditions, but this increase was not statistically significant (p-value > 0.05). Regardless of species-specific differences, both species showed the same trend of increased $\Phi_{e:C}/n_{PSII}$ and NPQ_{NSV} under iron limitation ([Table 1]()), which is consistent with our field observations. Furthermore, the
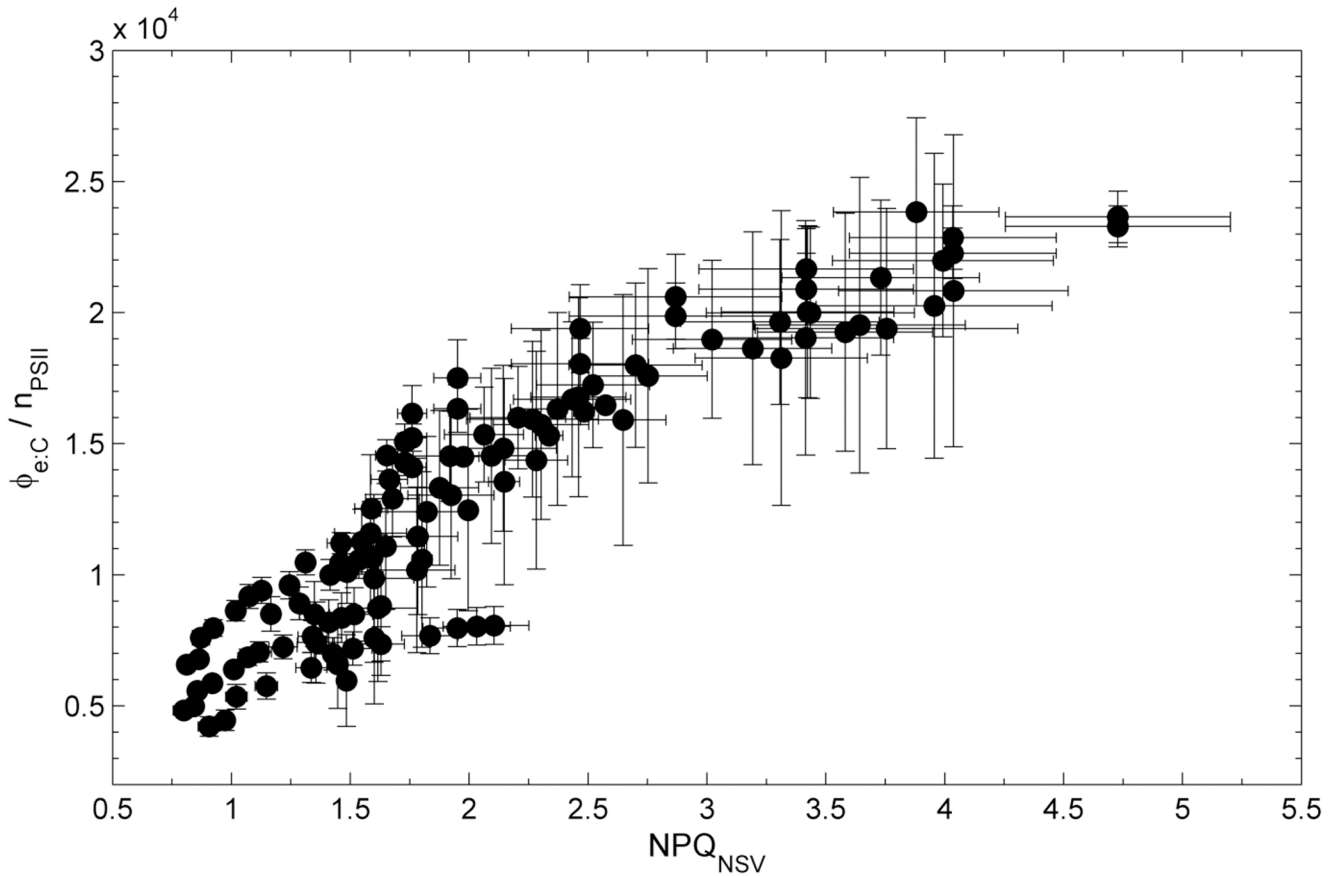
Fig 7. Relationship between the conversion factor $\Phi_{e:C}/n_{PSII}$ and NPQ_{NSV} values during the iron addition experiment. Values of $\Phi_{e:C}/n_{PSII}$ were derived from PvsE curves of CO_2-assimilation and ETR_{RCII} at irradiances corresponding to each ETR_{RCII}-PvsE curve light level. Units of $\Phi_{e:C}/n_{PSII}$ are (mol e$^-$ mol C^{-1}) / (mol chl a mol RCII^{-1}). NPQ_{NSV} values were derived as F_o'/F_v' for each light level of the SSLC. Data points represent means and standard errors for parameters derived from three biological replicates. A quadratic fit through all data points ($\Phi_{e:C}/n_{PSII}$ = -733.21 NPQ^2+8792.4 NPQ– 1477.1) is statistically significant (R^2 = 0.70, p-value < 0.0001).

doi:10.1371/journal.pone.0133235.g007

Table 1. Effect of iron limitation on photophysiology in two mono-specific phytoplankton cultures grown in the laboratory.

	T. oceanica		*C. polylepis*	
[Fe]	42nM	0.13nM	42nM	1.28nM
μ (d^{-1})	1.27 ± 0.14 (n = 6)***	0.41 ± 0.09 (n = 5)	0.53 ± 0.12 (n = 5)**	0.27 ± 0.05 (n = 4)
F_v/F_m	0.63 ± 0.01***	0.43 ± 0.01	0.51 ± 0.02**	0.41 ± 0.03
σ_{PSII}	643 ± 3	742 ± 16	591 ± 7	621 ± 3
P_{max} CO_2-assimilation	0.030 ± 0.004	0.035 ± 0.005	0.032 ± 0.009	0.028 ± 0.009
P_{max} ETR_{PSII}	174 ± 9*	330 ± 21	370 ± 26 *	506 ± 65
P_{max} $\Phi_{e:C}/n_{PSII}$	5874 ± 648*	9225 ± 1502	11691 ± 3730	18145 ± 6091
NPQ_{NSV}	0.37–0.47***	0.58–0.75	0.5–0.59***	0.72–0.79

* p-value< 0.05

** p-value< 0.01

***p-value< 0.0001

doi:10.1371/journal.pone.0133235.t001

species-specific differences observed in our laboratory experiments are consistent with changes in phytoplankton assemblage composition observed in our iron addition experiment, where the abundance of diatoms (lower $\Phi_{e:C}/n_{PSII}$) was increased in the iron addition treatment and the abundance of prymnesiophytes (higher $\Phi_{e:C}/n_{PSII}$) was decreased (S2 Fig).

Thalassiosira oceanica and *Chrysochromulina polylepis* were grown in steady state iron-replete and iron-limited conditions. The mean growth rate μ, derived from successive measurements in semi-continuous batch cultures, is given in d^{-1}. The error is the SD of 3 biological replicates, and number of consecutive batch transfers (ca. 4 cell divisions per transfer) used to calculate growth rates are given in brackets. F_v/F_m and σ_{PSII} are values from cultures in the dark regulated state (10 min of 5 μmol quanta $m^{-2}s^{-1}$ at 730 nm), measured on the day of CO_2-assimilation experiments. The error is SD of 3 biological replicates. Changes in these parameters are statistically significant for *T. oceanica* (p-value < 0.0001) and *C. polylepis* (p-value < 0.01). P_{max} for CO_2-assimilation (mol C mol chla^{-1} s^{-1}) and ETR_{RCII} (mol e- mol $RCII^{-1}$ s^{-1}) were derived from PvE curves as described in the methods section. The error is the 95% confidence interval of the P_{max} derived from the fit to data from 6 whole curve measurements (duplicate curves each from 3 biological replicates). The conversion factor $\Phi_{e:C}/n_{PSII}$ for P_{max} was derived as the quotient of P_{max} for ETR_{RCII} and P_{max} for CO_2-assimilation. The error is the propagated error from numerator and denominator. NPQ_{NSV} was estimated as F_o'/F_v' from the last ST acquisition during each light level of the PvE curves. The values shown are from the first and last step of the PvE curves (4 and 800 μmol quanta m^{-2} s^{-1}). Each NPQ_{NSV} value is the mean of 2 values measured on 3 biological replicates. Changes in response to iron limitation are statistically significant for both species (p-value < 0.0001).

Discussion

Our results provide new insight into the effects of iron and light availability on the coupling between CO_2-assimilation and photosynthetic electron transport in natural phytoplankton assemblages and mono-specific laboratory cultures. We show that both of these environmental variables significantly influence $\Phi_{e:C}/n_{PSII}$, which has important implications for the use of FRRF measurements to infer rates of CO_2-assimilation in oceanic waters. Below, we first discuss the observed increase in $\Phi_{e:C}/n_{PSII}$ under excess light and low iron conditions in the context of previously reported values. We then discuss the effects of iron and light on phytoplankton photophysiology, and suggest a simple conceptual explanation for the observed increase in ETR_{RCII} under iron limitation. We hypothesize, that iron and light-dependent changes in $\Phi_{e:C}/n_{PSII}$ are driven by the need to dissipate excess excitation energy, caused by either excess light, or the effects of iron limitation on the ETC. In this context, we discuss the correlation between $\Phi_{e:C}/n_{PSII}$ and NPQ_{NSV}, and examine the potential significance of this finding in the context of marine primary productivity studies.

Magnitude of the observed conversion factor

The conversion factor $\Phi_{e:C}/n_{PSII}$, derived from our measurements of ETR_{RCII} and CO_2-assimilation, varied significantly in response to light and iron availability. In our field experiment, the addition of iron caused the value of $\Phi_{e:C}/n_{PSII}$ at light saturation (P_{max}) to decrease by 66% within 6 days (Fig 4F). Furthermore, short-term changes in light availability had a major effect on the value of $\Phi_{e:C}/n_{PSII}$, and this effect was enhanced under iron limitation. A recent meta-analysis of variability in experimentally determined $\Phi_{e:C}$ from 14 field studies found values ranging from 1.15 to 54.2 with a mean of 10.9 ± 6.91 mol e$^-$ mol C^{-1} [24]. This analysis comprised a wide range of oceanic regions, but did not include observations from the NE subarctic Pacific or other HNLC regions. Due to our experimental approach, we are unable to derive

absolute values for $\Phi_{e:C}$. However, if we assume $1/n_{PSII}$ to be 500 mol chl$a$ mol RCII^{-1} [20], as has been done in most previous studies [24], $\Phi_{e:C}$ values on day 3 of the iron-addition experiment range from 13 to 39 mol e$^-$ mol C^{-1}. Using a constant value of $1/n_{PSII}$ for both treatments is unlikely to be realistic. Even though iron-limited phytoplankton possess less chl a per cell, $1/n_{PSII}$, the ratio of chl a to RCII, has frequently been observed to increase under low iron conditions [84,85,88,90,98]. If we thus assume 700 mol chl a mol RCII^{-1} for the iron-limited control treatment and 500 mol chl a mol RCII^{-1} for the iron addition treatment [85], $\Phi_{e:C}$ ranges from 13 to 28 mol e$^-$ mol C^{-1}. These $\Phi_{e:C}$ values represent the range observed across different irradiance levels in our PvsE experiments. At the time of sampling, cells in the on board incubator were exposed to ~ 40 µmol quanta m^{-2} s^{-1}. Assuming 700 and 500 mol chl a mol RCII^{-1} for the iron-limited and iron-replete treatments, respectively, we derive $\Phi_{e:C}$ values of ~18 and ~15 mol e$^-$ mol C^{-1}. Values of $\Phi_{e:C}$ estimated from our data are thus within the range reported in previous field studies [24], with no estimate falling below the theoretical minimum of 4 mol e$^-$ mol C^{-1}.

Ideally, measurements of ETR$_{RCII}$ and CO$_2$-assimilation should be performed simultaneously on the same sample, eliminating differences in incubation time and spectral quality of the light sources used. As discussed in detail in the supplementary material, the differences in spectral distribution of the light sources used for FRRF and ^{14}C measurements could have led to an underestimation of absolute values of $\Phi_{e:C}/n_{PSII}$ (S1 Fig). However, these differences cannot explain the large iron dependent changes we observed in $\Phi_{e:C}/n_{PSII}$, since the absorption spectra of iron-limited and iron-enriched treatments did not differ drastically (S1 Fig). Furthermore, differences in incubation times could have influence the absolute magnitude of the derived conversion factor. Incubation times used for the PvsE curves were ca. 5 min for FRRF measurements (applied incrementally to the same sample), vs. 3–4 hours in the field and 30 min in the laboratory for ^{14}C-assimilation experiments (light levels applied simultaneously to different samples). As has been shown by Halsey et al. [16,17,99] and Pei and Laws [18], the use of fixed incubation times for cells growing at different growth rates could lead to an overestimation of our conversion factor $\Phi_{e:C}/n_{PSII}$ in the iron-limited relative to iron-replete samples. Additionally, the longer incubation time in CO$_2$-assimilation experiments might have exacerbated cumulative processes such as photodamage under excess irradiance. To address this issue, we did not utilize the part of the PvsE curves showing photo-inhibition. However, we cannot rule out any differential cumulative effects of photoinhibition on ETR$_{RCII}$ and ^{14}C-assimilation at P$_{max}$. This could potentially decrease CO$_2$-assimilation at P$_{max}$ relative to ETR$_{RCII}$ at P$_{max}$ and lead to overestimation of our $\Phi_{e:C}/n_{PSII}$ values at P$_{max}$. Notwithstanding these potential sources of uncertainty in the absolute value of $\Phi_{e:C}/n_{PSII}$, the good agreement between our estimated $\Phi_{e:C}$ (assuming ~ 500–700 mol chl a mol RCII^{-1}) and those of previous studies suggests that our observations are robust. More importantly, potential offsets in the absolute values of $\Phi_{e:C}/n_{PSII}$ do not diminish the significance of the relative, iron and light-dependent changes we observed in this parameter (discussed below).

Interacting effects of iron and light on the conversion factor $\Phi_{e:C}/n_{PSII}$

Our data show strong and interacting effects of iron and light availability on the conversion factor $\Phi_{e:C}/n_{PSII}$ in phytoplankton field assemblages and mono-specific laboratory cultures (Fig 4C, 4f and 6,Table 1). It has been shown that the magnitude of both $1/n_{PSII}$ and $\Phi_{e:C}$ vary significantly between phytoplankton taxa (e.g. [22,93]). Changes in $\Phi_{e:C}/n_{PSII}$ in field experiments was thus likely influenced by both, physiological changes and taxonomic shifts. These two sources of variability are, to a large extent, intrinsically linked, since changes in phytoplankton community composition (S2 Fig) reflect the selection of better adapted species under

any particular set of environmental conditions (i.e. iron limitation). In the following, we discuss the observed changes in $\Phi_{e:C}/n_{PSII}$ from a predominantly photophysiological point of view, since our laboratory results specifically demonstrate such physiological effects.

Numerous metabolic processes, acting between ETR_{RCII} and CO_2-assimilation can act to increase $\Phi_{e:C}$, and therefore the conversion factor $\Phi_{e:C}/n_{PSII}$ (e.g. [61,59,100]). In addition to its role in reducing CO_2 to organic carbon products, reductant (NADPH) formed at the end of the ETC can also be used for nitrate and sulphate reduction [101], photorespiration [102], or respiration via the malate shunt [103]. These alternative pathways decouple ETR_{RCII} from CO_2-assimilation, increasing the value of $\Phi_{e:C}$. Similarly, before the formation of NADPH, pseudo-cyclic electron flow can reduce O_2 and create a water-water cycle of electron transport, also increasing $\Phi_{e:C}$ (e.g. [104]). Pseudo-cyclic electron transport pathways can divert electrons from the ETC before (short water-water cycling, e.g. [105]) or after PSI (Mehler-reaction, e.g. [106]). Cyclic electron transport (CET) around PSII [107,108] and charge recombination in PSII [109,110], act more closely to the initial charge separation in RCII, and can also cause an increase in $\Phi_{e:C}$.

We suggest that the higher $\Phi_{e:C}/n_{PSII}$ observed in response to iron limitation and short-term increases in incident irradiance during the P*vs*E experiments (Fig 6A–6E) results predominantly from increases in the alternative electron flow pathways prior to reductant formation. These pathways, which are diagramed conceptually in Fig 8, can act as 'safety valves' to keep the primary quinone acceptor Q_A oxidized when excitation pressure on the ETC is high, thereby decreasing the potential of damage to RCII [111,54,55,61,56,104,112,60].

Iron limitation directly affects the photosynthetic ETC and thereby modulates the light-dependent changes in the conversion factor $\Phi_{e:C}/n_{PSII}$ (Fig 6A–6E). Importantly, iron limitation has been shown to alter the stoichiometry of ETC components (i.e. expression of iron-rich PSI and cytochrome b_6f complexes is down-regulated to a higher extent than PSII) (e.g. [62,84,116–118]). Low levels of electron acceptors downstream of PSII ultimately restrict the flow of electrons away from PSII during light exposure. This exacerbates the need for short (i.e. acting before PSI) alternative electron flow pathways to dissipate excess excitation energy and prevent over-reduction of RCII (Fig 8). A number of recent studies have suggested that re-routing electrons to a midstream plastoquinol oxidase (PTOX) to bypass the electron flow bottleneck of PSI is a common strategy in open ocean phytoplankton [113,55,54,56–58,62]. Importantly, up-regulation of pseudo-cyclic electron flow under iron limitation not only protects RCIIs from photodamage, but also helps to maintain a high ΔpH across the thylakoid membrane, providing energy for cell maintenance and growth [62,119]. Cyclic electron flow around PSII [107,108,114,61,120] and increases in charge recombination at PSII [109,110,115] are two additional mechanisms that can act to prevent over-reduction and damage of RCII when excitation pressure is high and the electron flow bottleneck is prior to PSI. Unlike PTOX-mediated water-water cycling, these processes do not contribute to an increase in ΔpH across the thylakoid membrane. They would, however, contribute to a high ETR_{RCII} and therefore $\Phi_{e:C}/n_{PSII}$ (Fig 8).

While ambient light intensity has a well-documented effect on values of $1/n_{PSII}$, these changes act on timescales longer than those of short-term P*vs*E experiments, and are thus unlikely to have caused the light-dependent changes we observed in $\Phi_{e:C}/n_{PSII}$ (Fig 6). On longer time-scales, however, iron limitation causes a reduction of chl *a* per cell (chlorosis), and an increase in chl *a* per functional RCII ($1/n_{PSII}$) [87,90]. This well documented response, which has been attributed to preferential down-regulation of RCII [87], and up-regulation of iron-stress-induced light harvesting complexes (isiLHCs) [62,90], would act to further increase $\Phi_{e:C}/n_{PSII}$ under iron limitation, regardless of light intensity (Fig 6A–6E).
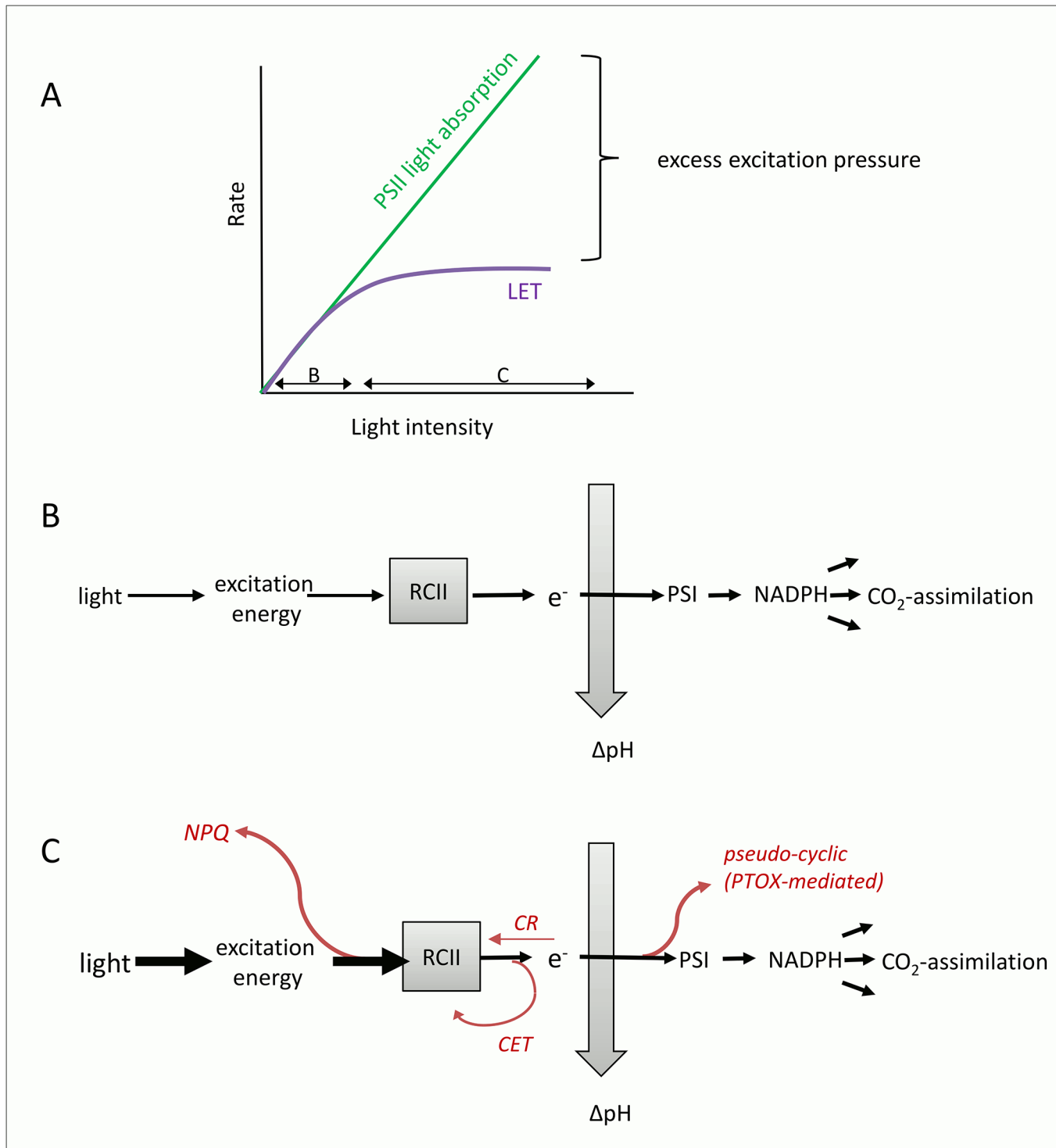
Fig 8. Conceptual diagram visualizing the concept of excess excitation pressure and its dissipation before and after charge separation in RCII. (A) Absorption of light energy by pigments in the light harvesting antenna of PSII cannot be controlled biologically, and rises linearly with incident light intensity. However, rates of linear electron transport (LET) and CO_2-assimilation saturate at a light intensity determined by the physiological state of the phytoplankton, resulting in a typical PvsE curve. Under optimal growth conditions, it is the resupply of NADP$^-$(predominantly from CO_2-assimilation) which limits LET, while under short-term exposure to excess light and under iron limitation, the 'bottleneck' of LET will be located before PSI. Whenever exitonic influx exceeds the chemical outflux at the level of RCII, excess excitation pressure needs to be safely dissipated to prevent photodamage. (B) Under optimal growth conditions and sub-saturating light, all absorbed photons are used for charge separation in RCII, and the majority of electrons will be used for LET and CO_2-assimilation, resulting in minimum $\Phi_{e:C}$. (C) Conditions of high excitation pressure can be caused by short-term exposure to high light, but also by iron limitation, which

comprises the functioning of the ETC and has been shown to create a 'bottle neck' for LET before PSI. Under these conditions, PTOX-mediated pseudo-cyclic electron flow (e.g. [54]–[58],[62],[105],[113]), cyclic electron transport around PSII (e.g. [107],[108],[114]), and charge recombination in RCII (e.g. [109],[110],[115]), have been suggested to safely dissipate excess excitation energy after RCII (but before PSI). Up-regulation of these alternative electron flow pathways could explain the high ETR_{RCII} (and $\Phi_{e:C}/n_{PSII}$) observed in our iron-limited samples. Excess excitation energy can also be dissipated in the light harvesting antenna, before charge separation in RCII. Collectively, a number of different molecular processes dissipating excess excitation energy in the PSII antenna can be quantified as NPQ_{NSV}.

In summary, we suggest that it is the effect of high excitation pressure, which causes a decoupling of ETR_{RCII} and CO_2-assimilation. This high excitation pressure may be a result of short-term exposure to excess irradiance as well as the effect of iron limitation on the ETC. This purely photophysiological interpretation can be extended to observations made in mixed phytoplankton communities. Here, fluctuating light and low iron conditions will select for species with the best ability to control high excitation pressure by adjusting the flow of excitation energy into, and the flow of electrons out of PSII.

Iron limitation increases ETR_{RCII}

To our knowledge, this is the first study which shows that ETR_{RCII} increases under iron limitation. This observation may seem counter-intuitive, and it is important to emphasize that our results do not imply an overall increase in photosynthetic electron transport under low iron conditions. Rather, our observations point to an increase in the rate of charge separation at each individual RCII, independent of the reduced total cellular concentration of these RCII. We show that the overall efficiency of PSII photochemistry in the light-regulated state, F_q'/F_m' (= Φ_{PSII}'), is reduced under iron limitation (Fig 5C), as expected. However, deconvolution of this parameter into its constituents F_q'/F_v' (Fig 5A) and F_v'/F_m' (Fig 5B) shows that F_q'/F_v', representing the fraction of open RCII (Q_A oxidized) at each given light level, increased under iron limitation. We hypothesize that this is likely achieved by increased alternative electron transport pathways acting to keep RCIIs open (Q_A oxidized) and bypassing the electron flow bottleneck at PSI, when excitation pressure is high (Fig 8). In contrast to F_q'/F_v', the parameter F_v'/F_m' is much lower when iron is limiting (Fig 5B), indicating that the excitation energy transfer in the antennae is compromised.

Based on our experimental observations, we suggest a simple mechanistic explanation for the observed increase in ETR_{RCII} under iron limitation. Cellular iron demand can be significantly reduced by economizing on iron-rich components of the photosynthetic apparatus and 'funneling' more electrons down fewer RCIIs (i.e., increasing ETR_{RCII}). In line with this explanation is the observation that values of σ_{PSII} are high under iron limitation, and rapidly decrease after iron addition (Fig 2) [121],[122],[84],[85],[123]–[126],[87]. Strzepek et al. [127] suggested that increased σ_{PSII} compensates for fewer iron-rich photosynthetic reaction centers in Southern Ocean phytoplankton species. Similarly, Ryan-Keogh et al. [128] noted that increasing the absorption cross section of RCs by the expression of isiLHCs allows cells to reduce the cellular iron requirement while maintaining the same light absorption capacity.

In conclusion, our results and interpretation support a scenario where photosynthetic electron flow has been fine-tuned to maximize energy conversion as well as photo-protection under conditions where ETC component abundance and stoichiometry are compromised by the availability of iron.

Link to NPQ_{NSV}

Above, we discussed how mechanisms acting down-stream of the initial charge separation in RCII are likely to be enhanced under conditions of high excitation pressure, resulting in high

ETR_{RCII} and $\Phi_{e:C}/n_{PSII}$. High excitation pressure can also be dissipated in the pigment antenna, before reaching RCII [104]. Fig 8 shows schematically the 'safety mechanisms' used for the dissipation of excess energy at both sides of RCII. Because processes dissipating excess excitation pressure in the antenna also quench ChlF yields measured by FRRF, they have collectively been called non-photochemical quenching (NPQ). NPQ, which is present in all oxygenic photosynthetic organisms, encompasses a wide variety of mechanisms acting to dissipate absorbed light energy as heat before it reaches RCII [129–134]. Following the approach of McKew et al.[80], we estimated NPQ from FRRF measurements as so-called normalized Stern-Volmer quenching (NPQ_{NSV}). We observed a strong correlation between the conversion factor $\Phi_{e:C}/n_{PSII}$ and the expression of NPQ_{NSV} (Fig 7). We note that $\Phi_{e:C}/n_{PSII}$ and NPQ_{NSV} are not entirely independent parameters, and therefore the strong correlation observed in Fig 7 is in part a result of their co-dependence on the ChlF parameter $F_v{}'$ (which we used in the derivation of both NPQ_{NSV} and $\Phi_{e:C}/n_{PSII}$).

At this point, the relationship between $\Phi_{e:C}/n_{PSII}$ and NPQ_{NSV} shown in Fig 7 is empirical rather than mechanistic. However, while there are a number of processes which will influence $\Phi_{e:C}/n_{PSII}$ and NPQ_{NSV} differentially, there are many processes related to the amount of excitation pressure experienced by the ETC that would influence both in a consistent manner. Numerous studies have shown that $\Phi_{e:C}$ increases if light is saturating, i.e. when excitation pressure is high (e.g. [33,36,40]). Clearly, excess light would also increase the expression of NPQ_{NSV}. Indeed, very recent work has pointed to a mechanistic link between alternative electron sinks involving PTOX and the expression of NPQ_{NSV} [105].

A possible approach towards improved prediction of CO_2-assimilation from FRRF data

While it remains to be seen how strong the correlation between $\Phi_{e:C}/n_{PSII}$ and NPQ_{NSV} (Fig 7) may be for other datasets, our results provide a potential basis for improved estimates of CO_2-assimilation from FRRF measurements alone. A number of factors make this approach more desirable than the use of static, regional conversion factors. First, the magnitude of $\Phi_{e:C}/n_{PSII}$ in phytoplankton assemblages will be determined by a multitude of interacting environmental variables. The use of NPQ_{NSV} as an integrated physiological measure of environmental effects on electron transport processes will therefore help to constrain the relationship between $\Phi_{e:C}/n_{PSII}$ and various environmental stressors. Secondly, as our data show, the magnitude of $\Phi_{e:C}/n_{PSII}$ can vary significantly within the same sample in response to short-term variations in incident light. Such small scale changes would be lost using a static (regional) conversion factor, but are captured with our NPQ_{NSV}-based approach, as every single ETR_{RCII} estimate is paired with a corresponding NPQ_{NSV} estimate. Finally, a non-static conversion factor is crucial if the goal is to monitor the effects of environmental change on marine primary productivity, since physiological responses to environmental change will likely affect the conversion factor itself before productivity changes are observed.

As a test of the validity of our approach, we used the $\Phi_{e:C}/n_{PSII}$ vs. NPQ_{NSV} correlation determined from our iron addition experiment (Fig 7) to predict the CO_2-assimilation rates from FRRF-derived ETR_{RCII} and NPQ_{NSV} measured along the Line-P transect. In this case, in situ phytoplankton assemblages were collected from within and below the mixed layer, and rate measurements were conducted immediately after collection, without any experimental manipulation (see methods). As shown in Fig 9, we obtained a strong correlation between the predicted and measured CO_2-assimilation rates (Spearman's $r = 0.90$, n = 95 and two-tailed p-value < 0.0001 on non log-transformed data). Our approach consistently underestimates values from the deepest sampling depth, which can likely be attributed to the lack of spectral
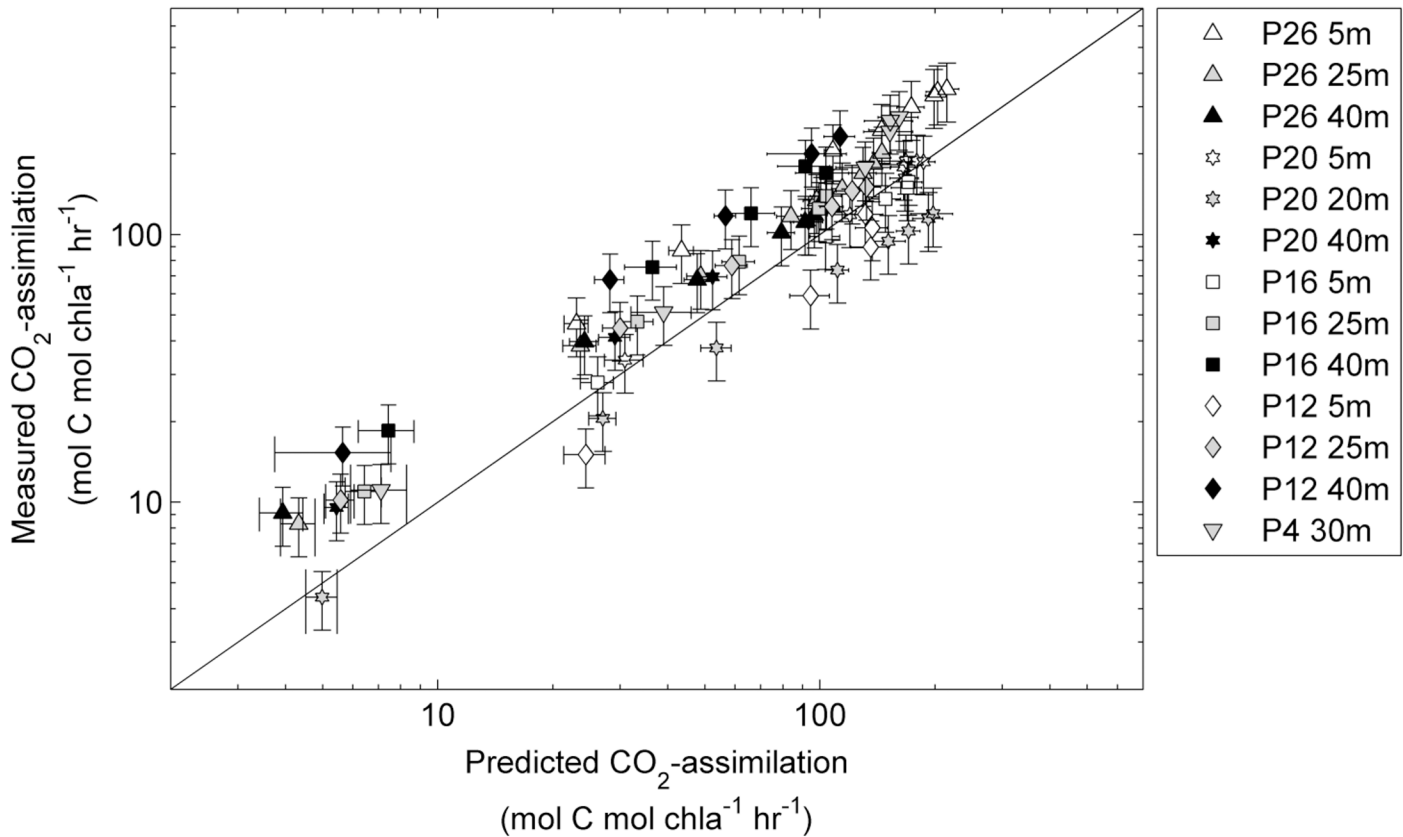
Fig 9. Rates of CO_2-assimilation (mol C mol chl a^{-1} hr^{-1}) derived from FRRF measurements plotted against rates measured by ^{14}C-assimilation experiments. Samples were taken at one to three depths at five stations along Line-P in the NE subarctic Pacific (see Fig 1). FRRF based PvsE curves were used to derive ETR_{RCII} and NPQ_{NSV} at 8 light levels for each sample, and $\Phi_{e:C}/n_{PSII}$ values were then derived from the relationship presented in Fig 7. $\Phi_{e:C}/n_{PSII}$ and ETR_{RCII} for each light level were used to calculate CO_2-assimilation rates. Error bars for predicted CO_2-assimilation rates represent the propagated error from the ChlF yields of the last three ST acquisitions of each light level during the FRRF PvsE curve used to derive NPQ_{NSV} and ETR_{RCII}. Error bars for measured CO_2-assimilation rates represent the mean coefficient of variance derived from all duplicate measurements (n = 46). The correlation between all predicted and measured data points (n = 95) was statistically significant (Spearman's r = 0.90, two-tailed p-value < 0.0001). All statistics are for non log-transformed data.

doi:10.1371/journal.pone.0133235.g009

correction of our data. The RMSE for the values predicted using our approach and measured values is 48.4 mol C mol chl a^{-1} hr^{-1}. This error represents ~ 10% of the total range of values observed along the transect during this study, suggesting that rates of productivity can be predicted with reasonable accuracy. In comparison with our approach, computation of CO_2-assimilation from FRRF data assuming a constant $1/n_{PSII}$ value of 500 mol chl a mol $RCII^{-1}$ and 4 mol e^- mol C^{-1}, significantly under-predicts observed CO_2-assimilation rates (RMSE = 837.3 mol C mol chl a^{-1} hr^{-1}). Even if we use a constant conversion factor derived from the average of the $\Phi_{e:C}/n_{PSII}$ measured during our iron addition experiment, the model error remains larger compared to that derived using our variable, NPQ_{NSV}-based conversion factor (Fig 7). Our data therefore show significant potential in the application of a variable, NPQ_{NSV}-derived conversion factor and associated quantification of carbon uptake rates from FRRF data.

Conclusion

Deriving rates of phytoplankton CO_2-assimilation from bio-optical approaches like FRRF has the potential to provide estimates of primary production at unprecedented spatial and temporal resolution. High resolution measurements, covering large oceanic regions, are essential for

the monitoring and modelling of marine food webs and global biogeochemical cycles. Further, such measurements are indispensable for the development and validation of algorithms estimating global marine primary productivity from remote sensing.

Crucial to this approach is a sound characterization of the conversion factor between FRRF-derived ETR_{RCII} and primary productivity in carbon units. Our data demonstrate that the conversion factor varies significantly in response to iron and light availability in phytoplankton field assemblages and mono-specific laboratory cultures. We interpret the observed variability in the conversion factor $\Phi_{e:C}/n_{PSII}$ as a manifestation of the extreme photophysiological flexibility which evolved in phytoplankton to maximize growth under dynamic light and nutrient regimes [135,136]. We hypothesize that, to a large extent, changes in $\Phi_{e:C}/n_{PSII}$ represent a suite of coordinated photophysiological adjustments acting to balance light absorption with CO_2-assimilation under given environmental conditions. These will be manifested on the physiological as well as on the taxonomic level. On the taxonomic level, a low nutrient and / or fluctuating light environment will select for species with the best ability to control high excitation pressure by adjusting the flow of excitation energy into, and the flow of electrons out of PSII (manifested in changes of NPQ_{NSV}, $1/n_{PSII}$ and $\Phi_{e:C}$). Future studies will be needed to evaluate the relationship between NPQ_{NSV} and $\Phi_{e:C}/n_{PSII}$ in a number of oceanic regions in order to evaluate the potential for improved CO_2-assimilation estimates from FRRF data.

Supporting Information

S1 Fig. Spectral distribution of light sources used for FRRF and Photosynthetron assays, and absorption spectra of phytoplankton assemblages on day 6 of the iron-addition experiment. (a) The FRRF instrument used during this study contains LEDs with peak output at four wavelengths (445 nm, 470 nm, 503 nm, 530 nm). In our FRRF instrument, excitation as well as actinic background irradiance is applied from the same LEDs. (b) Spectral distribution of the LEDs used in the photosynthetron used for ^{14}C-uptake experiments. (c) Spectral overlap of the two light sources. The overlap is good in the region of maximal light absorption by photosynthetic pigment (ca. 450 nm). However, in direct comparison with the photosynthetron, the FRRF instrument provides a higher proportion of photons in the region > 480 nm. This could have led to an underestimation of ETR_{RCII} values relative to CO_2-assimilation values measured in the photosynthetron, resulting in an under-estimate of $\Phi_{e:C}/n_{PSII}$. In addition to knowledge of spectral differences in the light sources used (a-c), spectral correction of our data would require light absorption spectra of the phytoplankton assemblages examined. Relative absorption spectra of the phytoplankton communities on day 6 after iron-addition (measured using the quantitative filter technique [65]) are shown in (d-f). Spectra from 3 biological replicates of the control (d) and two biological replicates of the iron addition treatment (e) were averaged, and these spectra are shown together in panel (f). The results show relatively small changes in the relative light absorption between the two treatments, and it is unlikely that these changes would have significantly influenced the large iron and light-dependent effects in $\Phi_{e:C}/n_{PSII}$. Because we did not measure absorption spectra for all sampling points of the iron addition experiment and stations along the transect, we were unable to spectrally correct our data. Furthermore, because we are not deriving absolute values for $\Phi_{e:C}/n_{PSII}$, we did not apply a constant correction factor (estimated from e.g. the data shown in a-f). (TIFF)

S2 Fig. Phytoplankton assemblage composition on day 6 of the iron addition experiment. The taxonomic composition of phytoplankton assemblages (% of total chl *a*) was derived from HPLC analysis of accessory photosynthetic pigment. Average values are shown from three biological replicates for the iron-limited control and the iron addition treatment on day 6 of the

experiment. One to1.5 L of water were filtered on 25 mm GF/F and stored at -80°C until analysis. Pigments were extracted and quantified as described by Taylor et al. [137]. Pigment ratios were then used to estimate phytoplankton assemblage composition using CHEMTAX as described by Taylor et al. [137]. The initial pigment ratio matrix used for our data was taken from Lee et al. [138], table 5, which is specific to North Pacific phytoplankton isolates.
(TIFF)

S3 Fig. Response of volume normalized rates of CO_2-assimilation (mol C m^{-3} hr^{-1}) during the iron addition experiment. The rates were measured as a function of irradiance, and P*vs*E curves were fit with the exponential model of Webb et al. [74]. Shown are mean values from three biological replicates where error bars represent standard error of mean and are sometimes smaller than symbols. Results shown in this figure confirm a strong stimulatory effect of iron additions on primary productivity in the experimental bottles.
(TIFF)

Acknowledgments

Author Contributions

Conceived and designed the experiments: NS CS PDT MTM. Performed the experiments: NS CS CD. Analyzed the data: NS PDT MTM. Wrote the paper: NS PDT MTM.

References

1. Field CB, Behrenfeld MJ, Randerson JT, Falkowski P. Primary production of the biosphere: integrating terrestrial and oceanic components. Science. 1998; 281: 237–240. PMID: 9657713

2. Falkowski PG, Barber RT, Smetacek V. Biogeochemical Controls and Feedbacks on Ocean Primary Production. Science. 1998; 281: 200–206. doi: 10.1126/science.281.5374.200 PMID: 9660741

3. Beardall J, Raven JA. The potential effects of global climate change on microalgal photosynthesis, growth and ecology. Phycologia. 2004; 43: 26–40. doi: 10.2216/i0031-8884-43-1-26.1

4. Hays GC, Richardson AJ, Robinson C. Climate change and marine plankton. Trends Ecol Evol. 2005; 20: 337–344. doi: 10.1016/j.tree.2005.03.004 PMID: 16701390

5. Chavez FP, Messié M, Pennington JT. Marine Primary Production in Relation to Climate Variability and Change. Annu Rev Mar Sci. 2011; 3: 227–260. doi: 10.1146/annurev.marine.010908.163917

6. Moore JK, Doney SC, Glover DM, Fung IY. Iron cycling and nutrient-limitation patterns in surface waters of the World Ocean. Deep Sea Res Part II Top Stud Oceanogr. 2001; 49: 463–507.

7. Boyd PW, Jickells T, Law CS, Blain S, Boyle EA, Buesseler KO, et al. Mesoscale iron enrichment experiments 1993–2005: Synthesis and future directions. science. 2007; 315: 612–617. PMID: 17272712

8. Behrenfeld M, Westberry T, Boss E, O'Malley R, Siegel D, Wiggert J, et al. Satellite-Detected Fluorescence Reveals Global Physiology of Ocean Phytoplankton. Biogeosciences. 2009; 779–794.

9. Raven JA, Evans MCW, Korb RE. The role of trace metals in photosynthetic electron transport in O2-evolving organisms. Photosynth Res. 1999; 60: 111–150. doi: 10.1023/A:1006282714942

10. Briat J-F, Curie C, Gaymard F. Iron utilization and metabolism in plants. Curr Opin Plant Biol. 2007; 10: 276–282. doi: 10.1016/j.pbi.2007.04.003 PMID: 17434791

11. Yruela I. Transition metals in plant photosynthesis. Met Integr Biometal Sci. 2013; 5: 1090–1109. doi: 10.1039/c3mt00086a

12. Suggett DJ, MacIntyre HL, Kana TM, Geider RJ. Comparing electron transport with gas exchange: parameterising exchange rates between alternative photosynthetic currencies for eukaryotic phytoplankton. Aquat Microb Ecol. 2009; 56: 147–162.

13. Steeman-Nielsen ES. Measurement of the Production of Organic Matter in the Sea by means of Carbon-14. Nature. 1951; 167: 684–685. doi: 10.1038/167684b0 PMID: 14826912

14. Williams PJ le B, Thomas DN, Reynolds CS. Phytoplankton Productivity: Carbon Assimilation in Marine and Freshwater Ecosystems. John Wiley & Sons; 2008.

15. Marra J. Net and gross productivity: weighing in with 14C. Aquat Microb Ecol. 2009; 56: 123–131.

16. Halsey KH, Milligan AJ, Behrenfeld MJ. Physiological optimization underlies growth rate-independent chlorophyll-specific gross and net primary production. Photosynth Res. 2010; 103: 125–137. doi: 10.1007/s11120-009-9526-z PMID: 20066494

17. Halsey KH, Milligan AJ, Behrenfeld MJ. Linking Time-Dependent Carbon-Fixation Efficiencies in Dunaliella Tertiolecta (chlorophyceae) to Underlying Metabolic Pathways1. J Phycol. 2011; 47: 66–76. doi: 10.1111/j.1529-8817.2010.00945.x

18. Pei S, Laws EA. Does the 14C method estimate net photosynthesis? Implications from batch and continuous culture studies of marine phytoplankton. Deep Sea Res Part Oceanogr Res Pap. 2013; 82: 1–9. doi: 10.1016/j.dsr.2013.07.011

19. Genty B, Briantais J-M, Baker NR. The relationship between the quantum yield of photosynthetic electron transport and quenching of chlorophyll fluorescence. Biochim Biophys Acta BBA—Gen Subj. 1989; 990: 87–92. doi: 10.1016/S0304-4165(89)80016-9

20. Kolber Z, Falkowski PG. Use of Active Fluorescence to Estimate Phytoplankton Photosynthesis in Situ. Limnol Oceanogr. 1993; 38: 1646–1665. doi: 10.2307/2838443

21. Kolber ZS, Prášil O, Falkowski PG. Measurements of variable chlorophyll fluorescence using fast repetition rate techniques: defining methodology and experimental protocols. Biochim Biophys Acta BBA—Bioenerg. 1998; 1367: 88–106. doi: 10.1016/S0005-2728(98)00135-2

22. Suggett DJ, Moore CM, Geider RJ. Estimating aquatic productivity from active fluorescence measurements. Chlorophyll Fluoresc Aquat Sci Methods Appl. 2010; 103–127.

23. Huot Y, Babin M. Overview of Fluorescence Protocols: Theory, Basic Concepts, and Practice. In: Suggett DJ, Prášil O, Borowitzka MA, editors. Chlorophyll a Fluorescence in Aquatic Sciences: Methods and Applications. Springer Netherlands; 2010. pp. 31–74. Available: http://link.springer.com/chapter/10.1007/978-90-481-9268-7_3

24. Lawrenz E, Silsbe G, Capuzzo E, Ylöstalo P, Forster RM, Simis SGH, et al. Predicting the Electron Requirement for Carbon Fixation in Seas and Oceans. PLoS ONE. 2013; 8: e58137. doi: 10.1371/journal.pone.0058137 PMID: 23516441

25. Boyd PW, Aiken J, Kolber Z. Comparison of radiocarbon and fluorescence based (pump and probe) measurements of phytoplankton photosynthetic characteristics in the northeast Atlantic Ocean. Oceanogr Lit Rev. 1997; 44.

26. Barranguet C, Kromkamp J. Estimating primary production rates from photosynthetic electron transport in estuarine microphytobenthos. Mar Ecol-Prog Ser. 2000; 204: 39–52.

27. Gilbert M, Domin A, Becker A, Wilhelm C. Estimation of Primary Productivity by Chlorophyll a in vivo Fluorescence in Freshwater Phytoplankton. Photosynthetica. 2000; 38: 111–126. doi: 10.1023/A:1026708327185

28. Suggett D, Kraay G, Holligan P, Davey M, Aiken J, Geider R. Assessment of photosynthesis in a spring cyanobacterial bloom by use of a fast repetition rate fluorometer. Limnol Oceanogr. 2001; 46: 802–810.

29. Moore C, Suggett D, Holligan P, Sharples J, Abraham E, Lucas M, et al. Physical controls on phytoplankton physiology and production at a shelf sea front: a fast repetition-rate fluorometer based field study. Mar Ecol Prog Ser. 2003; 259: 29–45. doi: 10.3354/meps259029

30. Raateoja M, Seppl J, Kuosa H. Bio-optical modelling of primary production in the SW Finnish coastal zone, Baltic Sea: fast repetition rate fluorometry in Case 2 waters. Mar Ecol Prog Ser. 2004; 267: 9–26. doi: 10.3354/meps267009

31. Raateoja MP. Fast repetition rate fluorometry (FRRF) measuring phytoplankton productivity: a case study at the entrance to the Gulf of Finland, Baltic Sea. Boreal Environ Res. 2004; 9: 263–276.

32. Smyth TJ, Pemberton KL, Aiken J, Geider RJ. A methodology to determine primary production and phytoplankton photosynthetic parameters from Fast Repetition Rate Fluorometry. J Plankton Res. 2004; 26: 1337–1350. doi: 10.1093/plankt/fbh124

33. Corno G, Letelier RM, Abbott MR, Karl DM. Assesing Primary Production Variability in the North Pacific Subtropical Gyre: a Comparison of Fast Repetition Rate Fluorometry and 14C Measurements. J Phycol. 2006; 42: 51–60.

34. Estévez-Blanco P, Cermeño P, Espiñeira M, Fernández E. Phytoplankton photosynthetic efficiency and primary production rates estimated from fast repetition rate fluorometry at coastal embayments affected by upwelling (Rías Baixas, NW of Spain). J Plankton Res. 2006; 28: 1153–1165.

35. Suggett DJ, Maberly SC, Geider RJ. Gross photosynthesis and lake community metabolism during the spring phytoplankton bloom. Limnol Oceanogr. 2006; 2064–2076.

36. Kaiblinger C, Dokulil MT. Application of fast repetition rate fluorometry to phytoplankton photosynthetic parameters in freshwaters. Photosynth Res. 2006; 88: 19–30. PMID: 16847741

37. Melrose DC, Oviatt CA, OReilly JE, Berman MS. Comparisons of fast repetition rate fluorescence estimated primary production and 14C uptake by phytoplankton. Mar Ecol Prog Ser. 2006; 311: 37–46. doi: 10.3354/meps311037

38. Moore CM, Suggett DJ, Hickman AE, Kim YN, Tweddle JF, Sharples J, et al. Phytoplankton photoacclimation and photoadaptation in response to environmental gradients in a shelf sea. Limnol Oceanogr. 2006; 936–949.

39. Pemberton KL, Clarke KR, Joint I. Quantifying uncertainties associated with the measurement of primary production. Mar Ecol Prog Ser. 2006; 322: 51–59.

40. Fujiki T, Suzue T, Kimoto H, Saino T. Photosynthetic electron transport in Dunaliella tertiolecta (Chlorophyceae) measured by fast repetition rate fluorometry: relation to carbon assimilation. J Plankton Res. 2007; 29: 199–208.

41. Debes H, Gaard E, Hansen B. Primary production on the Faroe shelf: Temporal variability and environmental influences. J Mar Syst. 2008; 74: 686–697.

42. Goto N, Miyazaki H, Nakamura N, Terai H, Ishida N, Mitamura O. Relationships between electron transport rates determined by pulse amplitude modulated (PAM) chlorophyll fluorescence and photosynthetic rates by traditional and common methods in natural freshwater phytoplankton. Fundam Appl Limnol Arch Fr Hydrobiol. 2008; 172: 121–134. doi: 10.1127/1863-9135/2008/0172-0121

43. Hancke K, Hancke TB, Olsen LM, Johnsen G, Glud RN. Temperature Effects on Microalgal Photosynthesis-Light Responses Measured by O2 Production, Pulse-Amplitude-Modulated Fluorescence, and 14c Assimilation1. J Phycol. 2008; 44: 501–514. doi: 10.1111/j.1529-8817.2008.00487.x

44. Kromkamp JC, Dijkman NA, Peene J, Simis SGH, Gons HJ. Estimating phytoplankton primary production in Lake IJsselmeer (The Netherlands) using variable fluorescence (PAM-FRRF) and C-uptake techniques. Eur J Phycol. 2008; 43: 327–344.

45. Prieto L, Vaillancourt RD, Hales B, Marra J. On the relationship between carbon fixation efficiency and bio-optical characteristics of phytoplankton. J Plankton Res. 2008; 30: 43–56.

46. Robinson C, Tilstone GH, Rees AP, Smyth TJ, Fishwick JR, Tarran GA, et al. Comparison of in vitro and in situ plankton production determinations. Aquat Microb Ecol. 2009; 54: 13–34.

47. Tripathy SC, Ishizaka J, Fujiki T, Shibata T, Okamura K, Hosaka T, et al. Assessment of carbon- and fluorescence-based primary productivity in Ariake Bay, southwestern Japan. Estuar Coast Shelf Sci. 2010; 87: 163–173. doi: 10.1016/j.ecss.2010.01.006

48. Cheah W, McMinn A, Griffiths FB, Westwood KJ, Wright SW, Molina E, et al. Assessing Sub-Antarctic Zone primary productivity from fast repetition rate fluorometry. Deep Sea Res Part II Top Stud Oceanogr. 2011; 58: 2179–2188. doi: 10.1016/j.dsr2.2011.05.023

49. Fujiki T, Matsumoto K, Watanabe S, Hosaka T, Saino T. Phytoplankton productivity in the western subarctic gyre of the North Pacific in early summer 2006. J Oceanogr. 2011; 67: 295–303. doi: 10.1007/s10872-011-0028-1

50. Kromkamp JC, Peene J, Silsbe G. A comparison between primary production estimates based on fluorometry and C-fixation. European Journal of Phycology. Taylor & Francis, England; 2011. pp. 53–53.

51. Napoléon C, Claquin P. Multi-Parametric Relationships between PAM Measurements and Carbon Incorporation, an In Situ Approach. PloS One. 2012; 7: e40284. doi: 10.1371/journal.pone.0040284 PMID: 22911698

52. Napoléon C, Raimbault V, Claquin P. Influence of Nutrient Stress on the Relationships between PAM Measurements and Carbon Incorporation in Four Phytoplankton Species. PLoS ONE. 2013; 8: e66423. doi: 10.1371/journal.pone.0066423 PMID: 23805221

53. Robinson C, Suggett DJ, Cherukuru N, Ralph PJ, Doblin MA. Performance of Fast Repetition Rate fluorometry based estimates of primary productivity in coastal waters. J Mar Syst. 2014; doi: 10.1016/j.jmarsys.2014.07.016

54. Bailey S, Melis A, Mackey KRM, Cardol P, Finazzi G, van Dijken G, et al. Alternative photosynthetic electron flow to oxygen in marine Synechococcus. Biochim Biophys Acta BBA—Bioenerg. 2008; 1777: 269–276. doi: 10.1016/j.bbabio.2008.01.002

55. Cardol P, Bailleul B, Rappaport F, Derelle E, Béal D, Breyton C, et al. An original adaptation of photosynthesis in the marine green alga Ostreococcus. Proc Natl Acad Sci. 2008; 105: 7881–7886. doi: 10.1073/pnas.0802762105 PMID: 18511560

56. Mackey KRM, Paytan A, Grossman AR, Bailey S. A photosynthetic strategy for coping in a high-light, low-nutrient environment. Limnol Oceanogr. 2008; 53: 900–913. doi: 10.4319/lo.2008.53.3.0900

57. Zehr JP, Kudela RM. Photosynthesis in the Open Ocean. Science. 2009; 326: 945–946. doi: 10.1126/science.1181277 PMID: 19965502

58. Grossman AR, Mackey KRM, Bailey S. A Perspective on Photosynthesis in the Oligotrophic Oceans: Hypotheses Concerning Alternate Routes of Electron Flow1. J Phycol. 2010; 46: 629–634. doi: 10.1111/j.1529-8817.2010.00852.x

59. Peltier G, Tolleter D, Billon E, Cournac L. Auxiliary electron transport pathways in chloroplasts of microalgae. Photosynth Res. 2010; 106: 19–31. doi: 10.1007/s11120-010-9575-3 PMID: 20607407

60. McDonald AE, Ivanov AG, Bode R, Maxwell DP, Rodermel SR, Hüner NP. Flexibility in photosynthetic electron transport: the physiological role of plastoquinol terminal oxidase (PTOX). Biochim Biophys Acta BBA-Bioenerg. 2011; 1807: 954–967.

61. Cardol P, Forti G, Finazzi G. Regulation of electron transport in microalgae. Biochim Biophys Acta BBA-Bioenerg. 2011; 1807: 912–918.

62. Behrenfeld MJ, Milligan AJ. Photophysiological Expressions of Iron Stress in Phytoplankton. Annu Rev Mar Sci. 2013; 5. doi: 10.1146/annurev-marine-121211-172356

63. Halsey KH, Jones BM. Phytoplankton Strategies for Photosynthetic Energy Allocation. Annu Rev Mar Sci. 2015; 7: 265–297. doi: 10.1146/annurev-marine-010814-015813

64. Johnson KS, Miller LA, Sutherland NE, Wong CS. Iron transport by mesoscale Haida eddies in the Gulf of Alaska. Deep Sea Res Part II Top Stud Oceanogr. 2005; 52: 933–953. doi: 10.1016/j.dsr2.2004.08.017

65. Mitchell BG, Kahru M, Wieland J, Stramska M. Determination of spectral absorption coefficients of particles, dissolved material and phytoplankton for discrete water samples. Ocean Opt Protoc Satell Ocean Color Sens Valid Revis. 2002; 3: 231–257.

66. Booth BC. Size classes and major taxonomic groups of phytoplankton at two locations in the subarctic pacific ocean in May and August, 1984. Mar Biol. 1988; 97: 275–286. doi: 10.1007/BF00391313

67. Chappell PD, Whitney LP, Wallace JR, Darer AI, Jean-Charles S, Jenkins BD. Genetic indicators of iron limitation in wild populations of Thalassiosira oceanica from the northeast Pacific Ocean. ISME J. 2015; 9: 592–602. doi: 10.1038/ismej.2014.171 PMID: 25333460

68. Price NM, Harrison GI, Hering JG, Hudson RJ, Nirel PMV, Palenik B, et al. Preparation and Chemistry of the Artificial Algal Culture Medium Aquil. Biol Oceanogr. 1989; 6: 443–461. doi: 10.1080/01965581.1988.10749544

69. Maldonado MT, Allen AE, Chong JS, Lin K, Leus D, Karpenko N, et al. Copper-dependent iron transport in coastal and oceanic diatoms. Limnol Ocean. 2006; 51: 1729–1743.

70. Brand LE, Guillard RRL, Murphy LS. A method for the rapid and precise determination of acclimated phytoplankton reproduction rates. J Plankton Res. 1981; 3: 193–201. doi: 10.1093/plankt/3.2.193

71. Welschmeyer NA. Fluorometric analysis of chlorophyll a in the presence of chlorophyll b and pheopigments. Limnol Oceanogr. 1994; 39: 1985–1992.

72. Lewis M, Smith J. A small volume, short-incubation-time method for measurement of photosynthesis as a function of incident irradiance. Mar Ecol Prog Ser. 1983; 13: 99–102. doi: 10.3354/meps013099

73. Knap AH, Michaels A, Close AR, Ducklow H, Dickson AG. Protocols for the joint global ocean flux study (JGOFS) core measurements. JGOFS Repr IOC Man Guid No 29 UNESCO 1994. 1996;19. Available: http://epic.awi.de/17559/1/Kna1996a.pdf

74. Webb WL, Newton M, Starr D. Carbon Dioxide Exchange of Alnus rubra. A Mathematical Model. Oecologia. 1974; 17: 281–291.

75. Oxborough K, Baker NR. Resolving chlorophyll a fluorescence images of photosynthetic efficiency into photochemical and non-photochemical components–calculation of qP and Fv'/Fm'; without measuring Fo'; Photosynth Res. 1997; 54: 135–142. doi: 10.1023/A:1005936823310

76. Ruban AV, Murchie EH. Assessing the photoprotective effectiveness of non-photochemical chlorophyll fluorescence quenching: A new approach. Biochim Biophys Acta BBA—Bioenerg. 2012; 1817: 977–982. doi: 10.1016/j.bbabio.2012.03.026

77. Roháček K. Chlorophyll Fluorescence Parameters: The Definitions, Photosynthetic Meaning, and Mutual Relationships. Photosynthetica. 2002; 40: 13–29. doi: 10.1023/A:1020125719386

78. Kitajima M, Butler WL. Quenching of chlorophyll fluorescence and primary photochemistry in chloroplasts by dibromothymoquinone. Biochim Biophys Acta BBA—Bioenerg. 1975; 376: 105–115. doi: 10.1016/0005-2728(75)90209-1

79. Duysens LNM, Sweers HE. Studies on microalgae and photosynthetic bacteria. Jpn Soc Plant Physiol Univ Tokyo Tokyo. 1963;353.

80. McKew BA, Davey P, Finch SJ, Hopkins J, Lefebvre SC, Metodiev MV, et al. The trade-off between the light-harvesting and photoprotective functions of fucoxanthin-chlorophyll proteins dominates light acclimation in Emiliania huxleyi (clone CCMP 1516). New Phytol. 2013; 200: 74–85. doi: 10.1111/nph.12373 PMID: 23790241

81. Arrigo KR, Mills MM, Kropuenske LR, Dijken GL van, Alderkamp A-C, Robinson DH. Photophysiology in Two Major Southern Ocean Phytoplankton Taxa: Photosynthesis and Growth of Phaeocystis antarctica and Fragilariopsis cylindrus under Different Irradiance Levels. Integr Comp Biol. 2010; 50: 950–966. doi: 10.1093/icb/icq021 PMID: 21558252

82. Dubinsky Z, Falkowski PG, Wyman K. Light Harvesting and Utilization by Phytoplankton. Plant Cell Physiol. 1986; 27: 1335–1349.

83. Berges JA, Charlebois DO, Mauzerall DC, Falkowski PG. Differential Effects of Nitrogen Limitation on Photosynthetic Efficiency of Photosystems I and II in Microalgae. Plant Physiol. 1996; 110: 689–696. doi: 10.1104/pp.110.2.689 PMID: 12226211

84. Greene RM, Geider RJ, Falkowski PG. Effect of iron limitation on photosynthesis in a marine diatom. Limnol Oceanogr. 1991; 36: 1772–1782.

85. Greene RM, Geider RJ, Kolber Z, Falkowski PG. Iron-induced changes in light harvesting and photochemical energy conversion processes in eukaryotic marine algae. Plant Physiol. 1992; 100: 565–575. PMID: 16653030

86. Greene RM, Kolber ZS, Swift DG, Tindale NW, Falkowski PG. Physiological Limitation of Phytoplankton Photosynthesis in the Eastern Equatorial Pacific Determined from Variability in the Quantum Yield of Fluorescence. Limnol Oceanogr. 1994; 39: 1061–1074. doi: 10.2307/2838472

87. Vassiliev IR, Kolber Z, Wyman KD, Mauzerall D, Shukla VK, Falkowski PG. Effects of Iron Limitation on Photosystem II Composition and Light Utilization in Dunaliella tertiolecta. Plant Physiol. 1995; 109: 963–972. PMID: 12228645

88. Allen AE, LaRoche J, Maheswari U, Lommer M, Schauer N, Lopez PJ, et al. Whole-cell response of the pennate diatom Phaeodactylum tricornutum to iron starvation. Proc Natl Acad Sci. 2008; 105: 10438–10443. doi: 10.1073/pnas.0711370105 PMID: 18653757

89. Thamatrakoln K, Bailleul B, Brown CM, Gorbunov MY, Kustka AB, Frada M, et al. Death-specific protein in a marine diatom regulates photosynthetic responses to iron and light availability. Proc Natl Acad Sci. 2013; 110: 20123–20128. doi: 10.1073/pnas.1304727110 PMID: 24277817

90. Macey AI, Ryan-Keogh T, Richier S, Moore CM, Bibby TS. Photosynthetic protein stoichiometry and photophysiology in the high latitude North Atlantic. Limnol Oceanogr. 2014; 59: 1853–1864. doi: 10.4319/lo.2014.59.6.1853

91. Falkowski PG, Owens TG, Ley AC, Mauzerall DC. Effects of Growth Irradiance Levels on the Ratio of Reaction Centers in Two Species of Marine Phytoplankton. Plant Physiol. 1981; 68: 969–973. doi: 10.1104/pp.68.4.969 PMID: 16662035

92. Mauzerall D, Greenbaum NL. The absolute size of a photosynthetic unit. Biochim Biophys Acta BBA—Bioenerg. 1989; 974: 119–140. doi: 10.1016/S0005-2728(89)80365-2

93. Suggett DJ, MacIntyre HL, Geider RJ. Evaluation of biophysical and optical determinations of light absorption by photosystem II in phytoplankton. Limnol Ocean Methods. 2004; 2: 316–332.

94. Oxborough K, Moore CM, Suggett DJ, Lawson T, Chan HG, Geider RJ. Direct estimation of functional PSII reaction center concentration and PSII electron flux on a volume basis: a new approach to the analysis of Fast Repetition Rate fluorometry (FRRf) data. Limnol Ocean Methods. 2012; 10: 142–154.

95. Greg M. Silsbe KO. Toward autonomous measurements of photosynthetic electron transport rates: An evaluation of active fluorescence-based measurements of photochemistry. Limnol Oceanogr Methods. 2015; 13. doi: 10.1002/lom3.10014

96. Marchetti A, Sherry ND, Juneau P, Strzepek RF, Harrison PJ. Phytoplankton processes during a mesoscale iron enrichment in the NE subarctic Pacific: Part III—Primary productivity. Deep Sea Res Part II Top Stud Oceanogr. 2006; 53: 2131–2151.

97. Geider RJ, Roche JL. The role of iron in phytoplankton photosynthesis, and the potential for iron-limitation of primary productivity in the sea. Photosynth Res. 1994; 39: 275–301. doi: 10.1007/BF00014588 PMID: 24311126

98. Greene RM, Kolber ZS, Swift DG, Tindale NW, Falkowski PG. Physiological limitation of phytoplankton photosynthesis in the eastern equatorial Pacific determined from variability in the quantum yield of fluorescence. Limnol Oceanogr. 1994; 1061–1074.

99. Halsey KH, O'Malley RT, Graff JR, Milligan AJ, Behrenfeld MJ. A common partitioning strategy for photosynthetic products in evolutionarily distinct phytoplankton species. New Phytol. 2013; 198: 1030–1038. doi: 10.1111/nph.12209 PMID: 23452244

100. Rochaix JD. Regulation of photosynthetic electron transport. Biochim Biophys Acta BBA-Bioenerg. 2011; 1807: 375–383.

101. Laws EA. Photosynthetic quotients, new production and net community production in the open ocean. Deep Sea Res Part Oceanogr Res Pap. 1991; 38: 143–167.

102. Beardall J. Photosynthesis and photorespiration in marine phytoplankton. Aquat Bot. 1989; 34: 105–130. doi: 10.1016/0304-3770(89)90052-1

103. Scheibe R. Malate valves to balance cellular energy supply. Physiol Plant. 2004; 120: 21–26. doi: 10.1111/j.0031-9317.2004.0222.x PMID: 15032873

104. Niyogi KK. Safety valves for photosynthesis. Curr Opin Plant Biol. 2000; 3: 455–460. doi: 10.1016/S1369-5266(00)00113-8 PMID: 11074375

105. Nawrocki WJ, Tourasse NJ, Taly A, Rappaport F, Wollman F- A. The Plastid Terminal Oxidase: Its Elusive Function Points to Multiple Contributions to Plastid Physiology. Annu Rev Plant Biol. 2015; 66: null. doi: 10.1146/annurev-arplant-043014-114744

106. Miyake C, Asada K. The Water-Water Cycle in Algae. In: Larkum AWD, Douglas SE, Raven JA, editors. Photosynthesis in Algae. Springer Netherlands; 2003. pp. 183–204. Available: http://link.springer.com/chapter/10.1007/978-94-007-1038-2_9

107. Falkowski PG, Fujita Y, Ley A, Mauzerall D. Evidence for Cyclic Electron Flow around Photosystem II in Chlorella pyrenoidosa. Plant Physiol. 1986; 81: 310–312. PMID: 16664797

108. Prasil O, Kolber Z, Berry JA, Falkowski PG. Cyclic electron flow around Photosystem II <i>in vivo</i> Photosynth Res. 1996; 48: 395–410. doi: 10.1007/BF00029472

109. Ivanov AG, Sane PV, Hurry V, Öquist G, Huner NPA. Photosystem II reaction centre quenching: mechanisms and physiological role. Photosynth Res. 2008; 98: 565–574. doi: 10.1007/s11120-008-9365-3 PMID: 18821028

110. Vass I. Role of charge recombination processes in photodamage and photoprotection of the photosystem II complex. Physiol Plant. 2011; 142: 6–16. doi: 10.1111/j.1399-3054.2011.01454.x PMID: 21288250

111. Krause GH, Jahns P. Pulse Amplitude Modulated Chlorophyll Fluorometry and its Application in Plant Science. In: Green BR, Parson WW, editors. Light-Harvesting Antennas in Photosynthesis. Springer Netherlands; 2003. pp. 373–399. Available: http://link.springer.com/chapter/10.1007/978-94-017-2087-8_13

112. Ort DR, Baker NR. A photoprotective role for O2 as an alternative electron sink in photosynthesis? Curr Opin Plant Biol. 2002; 5: 193–198. doi: 10.1016/S1369-5266(02)00259-5 PMID: 11960735

113. Behrenfeld MJ, Halsey KH, Milligan AJ. Evolved physiological responses of phytoplankton to their integrated growth environment. Philos Trans R Soc B Biol Sci. 2008; 363: 2687–2703.

114. Onno Feikema W, Marosvölgyi MA, Lavaud J, van Gorkom HJ. Cyclic electron transfer in photosystem II in the marine diatom Phaeodactylum tricornutum. Biochim Biophys Acta BBA—Bioenerg. 2006; 1757: 829–834. doi: 10.1016/j.bbabio.2006.06.003

115. Vass I, Cser K. Janus-faced charge recombinations in photosystem II photoinhibition. Trends Plant Sci. 2009; 14: 200–205. doi: 10.1016/j.tplants.2009.01.009 PMID: 19303349

116. Strzepek RF, Harrison PJ. Photosynthetic architecture differs in coastal and oceanic diatoms. Nature. 2004; 431: 689–692. doi: 10.1038/nature02954 PMID: 15470428

117. Schrader PS, Milligan AJ, Behrenfeld MJ. Surplus Photosynthetic Antennae Complexes Underlie Diagnostics of Iron Limitation in a Cyanobacterium. PLoS ONE. 2011; 6: e18753. doi: 10.1371/journal.pone.0018753 PMID: 21533084

118. Fraser JM, Tulk SE, Jeans JA, Campbell DA, Bibby TS, Cockshutt AM. Photophysiological and Photosynthetic Complex Changes during Iron Starvation in Synechocystis sp. PCC 6803 and Synechococcus elongatus PCC 7942. Stal LJ, editor. PLoS ONE. 2013; 8: e59861. doi: 10.1371/journal.pone.0059861 PMID: 23527279

119. Laureau C, DE Paepe R, Latouche G, Moreno-Chacón M, Finazzi G, Kuntz M, et al. Plastid terminal oxidase (PTOX) has the potential to act as a safety valve for excess excitation energy in the alpine plant species Ranunculus glacialis L. Plant Cell Environ. 2013; doi: 10.1111/pce.12059

120. Shinopoulos KE, Brudvig GW. Cytochrome b559 and cyclic electron transfer within photosystem II. Biochim Biophys Acta BBA—Bioenerg. 2012; 1817: 66–75. doi: 10.1016/j.bbabio.2011.08.002

121. Babin M, Morel A, Claustre H, Bricaud A, Kolber Z, Falkowski PG. Nitrogen- and irradiance-dependent variations of the maximum quantum yield of carbon fixation in eutrophic, mesotrophic and oligotrophic marine systems. Deep Sea Res Part Oceanogr Res Pap. 1996; 43: 1241–1272. doi: 10.1016/0967-0637(96)00058-1

122. Boyd P., Abraham E. Iron-mediated changes in phytoplankton photosynthetic competence during SOIREE. Deep Sea Res Part II Top Stud Oceanogr. 2001; 48: 2529–2550. doi: 10.1016/S0967-0645(01)00007-8

123. Hopkinson BM, Mitchell BG, Reynolds RA, Wang H, Selph KE, Measures CI, et al. Iron limitation across chlorophyll gradients in the southern Drake Passage: Phytoplankton responses to iron addition and photosynthetic indicators of iron stress. Limnol Oceanogr. 2007; 52: 2540–2554. doi: 10.4319/lo.2007.52.6.2540

124. Kolber ZS, Barber RT, Coale KH, Fitzwateri SE, Greene RM, Johnson KS, et al. Iron limitation of phytoplankton photosynthesis in the equatorial Pacific Ocean. Nature. 1994; 371: 145–149.

125. Petrou K, Hassler CS, Doblin MA, Shelly K, Schoemann V, van den Enden R, et al. Iron-limitation and high light stress on phytoplankton populations from the Australian Sub-Antarctic Zone (SAZ). Deep Sea Res Part II Top Stud Oceanogr. 2011; 58: 2200–2211. doi: 10.1016/j.dsr2.2011.05.020

126. Timmermans KR, Davey MS, Wagt B van der, Snoek J, Geider RJ, Veldhuis MJW, et al. Co-limitation by iron and light of Chaetoceros brevis, C. dichaeta and C. calcitrans (Bacillariophyceae). Mar Ecol Prog Ser. 2001; 217: 287–297. doi: 10.3354/meps217287

127. Strzepek RF, Maldonado MT, Hunter KA, Frew RD, Boyd PW. Adaptive strategies by Southern Ocean phytoplankton to lessen iron limitation: Uptake of organically complexed iron and reduced cellular iron requirements. Limnol Oceanogr. 2011; 56: 1983–2002. doi: 10.4319/lo.2011.56.6.1983

128. Ryan-Keogh TJ, Macey AI, Cockshutt AM, Moore CM, Bibby TS. The Cyanobacterial Chlorophyll-Binding-Protein IsiA Acts To Increase The In Vivo Effective Absorption Cross-Section Of PSI Under Iron Limitation1. J Phycol. 2012; Available: http://onlinelibrary.wiley.com/doi/10.1111/j.1529-8817.2011.01092.x/full

129. Goss R, Lepetit B. Biodiversity of NPQ. J Plant Physiol. doi: 10.1016/j.jplph.2014.03.004

130. Horton P. Optimization of light harvesting and photoprotection: molecular mechanisms and physiological consequences. Philos Trans R Soc B Biol Sci. 2012; 367: 3455–3465. doi: 10.1098/rstb.2012.0069

131. Niyogi KK, Truong TB. Evolution of flexible non-photochemical quenching mechanisms that regulate light harvesting in oxygenic photosynthesis. Curr Opin Plant Biol. 2013; 16: 307–314. doi: 10.1016/j.pbi.2013.03.011 PMID: 23583332

132. Ruban AV, Johnson MP, Duffy CDP. The photoprotective molecular switch in the photosystem II antenna. Biochim Biophys Acta BBA—Bioenerg. 2012; 1817: 167–181. doi: 10.1016/j.bbabio.2011.04.007

133. Ruban AV. Evolution under the sun: optimizing light harvesting in photosynthesis. J Exp Bot. 2014; eru400. doi: 10.1093/jxb/eru400

134. Zaks J, Amarnath K, Sylak-Glassman EJ, Fleming GR. Models and measurements of energy-dependent quenching. Photosynth Res. 2013; 116: 389–409. doi: 10.1007/s11120-013-9857-7 PMID: 23793348

135. Laney SR. Seconds to hour scale photosynthetic responses in marine microalgae [Internet]. Thesis. 2006. Available: http://ir.library.oregonstate.edu/xmlui/handle/1957/3052

136. Mackey KRM. On the response of marine phytoplankton to changing nutrient and light conditions [Internet]. 2010.

137. Taylor RL, Semeniuk DM, Payne CD, Zhou J, Tremblay J-É, Cullen JT, et al. Colimitation by light, nitrate, and iron in the Beaufort Sea in late summer. J Geophys Res Oceans. 2013; 118: 3260–3277. doi: 10.1002/jgrc.20244

138. Lee YW, Park MO, Kim YS, Kim SS, Kang CK. Application of photosynthetic pigment analysis using a HPLC and CHEMTAX program to studies of phytoplankton community composition. J Korean Soc Ocean. 2011; 16: 117–124.